67. Brennand KJ, Simone A, Jou J, Gelboin-Burkhart C, Tran N, Sangar S, Li Y, Mu Y, Chen G, Yu D, McCarthy S, Sebat J, Gage FH: **Modelling schizophrenia using human induced pluripotent stem cells.** *Nature* 2011, 473(7346):221–225.
68. Horiuchi Y, Kano S, Ishizuka K, Cascella NG, Ishii S, Talbot CC Jr, Jaffe AE, Okano H, Pevsner J, Colantuoni C, Sawa A: **Olfactory cells via nasal biopsy reflect the developing brain in gene expression profiles: utility and limitation of the surrogate tissues in research for brain disorders.** *Neurosci Res* 2013, 77(4):247–250.
69. Bundo M, Toyoshima M, Okada Y, Akamatsu W, Ueda J, Nemoto-Miyauchi T, Sunaga F, Toritsuka M, Ikawa D, Kakita A, Kato M, Kasai K, Kishimoto T, Nawa H, Okano H, Yoshikawa T, Kato T, Iwamoto K: **Increased L1 retrotransposition in the neuronal genome in schizophrenia.** *Neuron* 2013, 81(2):306–313.
70. Higurashi N, Uchida T, Lossin C, Misumi Y, Okada Y, Akamatsu W, Imaizumi Y, Zhang B, Nabeshima K, Mori MX, Katsurabayashi S, Shirasaka Y, Okano H, Hirose S: **A human Dravet syndrome model from patient induced pluripotent stem cells.** *Mol Brain* 2013, 6:19.
71. Liu Y, Lopez-Santiago LF, Yuan Y, Jones JM, Zhang H, O'Malley HA, Patino GA, O'Brien JE, Rusconi R, Gupta A, Thompson RC, Natowicz MR, Meisler MH, Isom LL, Parent JM: **Dravet syndrome patient-derived neurons suggest a novel epilepsy mechanism.** *Ann Neurol* 2013, 74(1):128–139.
72. Jiao J, Yang Y, Shi Y, Chen J, Gao R, Fan Y, Yao H, Liao W, Sun XF, Gao S: **Modeling Dravet syndrome using induced pluripotent stem cells (iPSCs) and directly converted neurons.** *Hum Mol Genet* 2013, 22(21):4241–4252.
73. Imaizumi Y, Okano H: **Modeling human neurological disorders with induced pluripotent stem cells.** *J Neurochem* 2013. Nov 29. doi:10.1111/jnc.12625.
74. Corti O, Lesage S, Brice A: **What genetics tells us about the causes and mechanisms of Parkinson's disease.** *Physiol Rev* 2011, 91(4):1161–1218.
75. Valente EM, Abou-Sleiman PM, Caputo V, Muqit MM, Harvey K, Gispert S, Ali Z, Del Turco D, Bentivoglio AR, Healy DG, Albanese A, Nussbaum R, Gonzalez-Maldonado R, Deller T, Salvi S, Cortelli P, Gilks WP, Latchman DS, Harvey RJ, Dallapiccola B, Auburger G, Wood NW: **Hereditary early-onset Parkinson's disease caused by mutations in PINK1.** *Science* 2004, 304(5674):1158–1160.
76. Kitada T, Asakawa S, Hattori N, Matsumine H, Yamamura Y, Minoshima S, Yokochi M, Mizuno Y, Shimizu N: **Mutations in the parkin gene cause autosomal recessive juvenile parkinsonism.** *Nature* 1998, 392(6676):605–608.
77. Shimura H, Hattori N, Kubo S, Mizuno Y, Asakawa S, Minoshima S, Shimizu N, Iwai K, Chiba T, Tanaka K, Suzuki T: **Familial Parkinson disease gene product, parkin, is a ubiquitin-protein ligase.** *Nat Genet* 2000, 25(3):302–305.
78. Shiba-Fukushima K, Imai Y, Yoshida S, Ishihama Y, Kanao T, Sato S, Hattori N: **PINK1-mediated phosphorylation of the Parkin ubiquitin-like domain primes mitochondrial translocation of Parkin and regulates mitophagy.** *Sci Rep* 2012, 2:1002.
79. Geisler S, Holmstrom KM, Skujat D, Fiesel FC, Rothfuss OC, Kahle PJ, Springer W: **PINK1/Parkin-mediated mitophagy is dependent on VDAC1 and p62/SQSTM1.** *Nat Cell Biol* 2010, 12(2):119–131.
80. Ramirez A, Heimbach A, Grundemann J, Stiller B, Hampshire D, Cid LP, Goebel I, Mubaidin AF, Wriekat AL, Roeper J, Al-Din A, Hillmer AM, Karsak M, Liss B, Woods CG, Behrens MI, Kubisch C: **Hereditary parkinsonism with dementia is caused by mutations in ATP13A2, encoding a lysosomal type 5 P-type ATPase.** *Nat Genet* 2006, 38(10):1184–1191.
81. Klein C, Lohmann-Hedrich K: **Impact of recent genetic findings in Parkinson's disease.** *Curr Opin Neurol* 2007, 20(4):453–464.
82. Reinhardt P, Schmid B, Burbulla LF, Schondorf DC, Wagner L, Glatza M, Hoing S, Hargus G, Heck SA, Dhingra A, Wu G, Muller S, Brockmann K, Kluba T, Maisel M, Kruger R, Berg D, Tsytsyura Y, Thiel CS, Psathaki OE, Klingauf J, Kuhlmann T, Klewin M, Muller H, Gasser T, Scholer HR, Sterneckert J: **Genetic correction of a LRRK2 mutation in human iPSCs links parkinsonian neurodegeneration to ERK-dependent changes in gene expression.** *Cell Stem Cell* 2013, 12(3):354–367.
83. Ghebranious N, Ivacic L, Mallum J, Dokken C: **Detection of ApoE E2, E3 and E4 alleles using MALDI-TOF mass spectrometry and the homogeneous mass-extend technology.** *Nucleic Acids Res* 2005, 33(17):e149.
84. Singh PP, Singh M, Mastana SS: **Genetic variation of apolipoproteins in North Indians.** *Hum Biol* 2002, 74(5):673–682.
85. Liberopoulos E, Siamopoulos K, Elisaf M: **Apolipoprotein E and renal disease.** *Am J Kidney Dis* 2004, 43(2):223–233.
86. Corder EH, Saunders AM, Strittmatter WJ, Schmechel DE, Gaskell PC, Small GW, Roses AD, Haines JL, Pericak-Vance MA: **Gene dose of apolipoprotein E type 4 allele and the risk of Alzheimer's disease in late onset families.** *Science* 1993, 261(5123):921–923.
87. Miller JD, Ganat YM, Kishinevsky S, Bowman RL, Liu B, Tu EY, Mandal PK, Vera E, Shim JW, Kriks S, Taldone T, Fusaki N, Tomishima MJ, Krainc D, Milner TA, Rossi DJ, Studer L: **Human iPSC-based modeling of late-onset disease via progerin-induced aging.** *Cell Stem Cell* 2013, 13(6):691–705.
88. Forno LS: **Neuropathology of Parkinson's disease.** *J Neuropathol Exp Neurol* 1996, 55(3):259–272.
89. Spillantini MG, Crowther RA, Jakes R, Cairns NJ, Lantos PL, Goedert M: **Filamentous alpha-synuclein inclusions link multiple system atrophy with Parkinson's disease and dementia with Lewy bodies.** *Neurosci Lett* 1998, 251(3):205–208.
90. Aizawa E, Hirabayashi Y, Iwanaga Y, Suzuki K, Sakurai K, Shimoji M, Aiba K, Wada T, Tooi N, Kawase E, Suemori H, Nakatsuji N, Mitani K: **Efficient and accurate homologous recombination in hESCs and hiPSCs using helper-dependent adenoviral vectors.** *Mol Ther* 2012, 20(2):424–431.
91. Chang CJ, Bouhassira EE: **Zinc-finger nuclease-mediated correction of α-thalassemia in iPS cells.** *Blood* 2012, 120(19):3906–3914.
92. Miller JC, Tan S, Qiao G, Barlow KA, Wang J, Xia DF, Meng X, Paschon DE, Leung E, Hinkley SJ, Dulay GP, Hua KL, Ankoudinova I, Cost GJ, Urnov FD, Zhang HS, Holmes MC, Zhang L, Gregory PD, Rebar EJ: **A TALE nuclease architecture for efficient genome editing.** *Nat Biotechnol* 2011, 29(2):143–148.
93. Hockemeyer D, Wang H, Kiani S, Lai CS, Gao Q, Cassady JP, Cost GJ, Zhang L, Santiago Y, Miller JC, Zeitler B, Cherone JM, Meng X, Hinkley SJ, Rebar EJ, Gregory PD, Urnov FD, Jaenisch R: **Genetic engineering of human pluripotent cells using TALE nucleases.** *Nat Biotechnol* 2011, 29(8):731–734.
94. Fu Y, Foden JA, Khayter C, Maeder ML, Reyon D, Joung JK, Sander JD: **High-frequency off-target mutagenesis induced by CRISPR-Cas nucleases in human cells.** *Nat Biotechnol* 2013, 31(9):822–826.
95. Ran FA, Hsu PD, Wright J, Agarwala V, Scott DA, Zhang F: **Genome engineering using the CRISPR-Cas9 system.** *Nat Protoc* 2013, 8(11):2281–2308.
96. Ran FA, Hsu PD, Lin CY, Gootenberg JS, Konermann S, Trevino AE, Scott DA, Inoue A, Matoba S, Zhang Y, Zhang F: **Double nicking by RNA-guided CRISPR Cas9 for enhanced genome editing specificity.** *Cell* 2013, 154(6):1380–1389.
97. Tsuji S: **Genetics of neurodegenerative diseases: insights from high-throughput resequencing.** *Hum Mol Genet* 2010, 19(R1):R65–R70.
98. Mitsui J, Mizuta I, Toyoda A, Ashida R, Takahashi Y, Goto J, Fukuda Y, Date H, Iwata A, Yamamoto M, Hattori N, Murata M, Toda T, Tsuji S: **Mutations for Gaucher disease confer high susceptibility to Parkinson disease.** *Arch Neurol* 2009, 66(5):571–576.
99. Iwata A, Iwatsubo T: **Disease-modifying therapy for Alzheimer's disease: Challenges and hopes.** *Neurol Clin Neurosci* 2003, 1(2):49–54.
100. Mertens J, Stuber K, Wunderlich P, Ladewig J, Kesavan JC, Vandenberghe R, Vandenbulcke M, van Damme P, Walter J, Brustle O, Koch P: **APP processing in human pluripotent stem cell-derived neurons is resistant to NSAID-based gamma-secretase modulation.** *Stem Cell Rep* 2013, 1(6):491–498.
101. Storandt M, Balota DA, Aschenbrenner AJ, Morris JC: **Clinical and psychological characteristics of the initial cohort of the Dominantly Inherited Alzheimer Network (DIAN).** *Neuropsychology* 2014, 28(1):19–29.
102. Moulder KL, Snider BJ, Mills SL, Buckles VD, Santacruz AM, Bateman RJ, Morris JC: **Dominantly Inherited Alzheimer network: facilitating research and clinical trials.** *Alzheimers Res Ther* 2013, 5(5):48.
103. Cash DM, Ridgway GR, Liang Y, Ryan NS, Kinnunen KM, Yeatman T, Malone IB, Benzinger TL, Jack CR Jr, Thompson PM, Ghetti BF, Saykin AJ, Masters CL, Ringman JM, Salloway SP, Schofield PR, Sperling RA, Cairns NJ, Marcus DS, Xiong C, Bateman RJ, Morris JC, Rossor MN, Ourselin S, Fox NC, Dominantly Inherited Alzheimer N: **The pattern of atrophy in familial Alzheimer disease: volumetric MRI results from the DIAN study.** *Neurology* 2013, 81(16):1425–1433.

doi:10.1186/1756-6606-7-22
Cite this article as: Okano and Yamanaka: iPS cell technologies: significance and applications to CNS regeneration and disease. *Molecular Brain* 2014 7:22.

OPEN ACCESS Freely available online

PLOS | ONE

Neural Substrates of Cognitive Subtypes in Parkinson's Disease: A 3-Year Longitudinal Study

Yumiko Shoji[1], Yoshiyuki Nishio[1]*, Toru Baba[1], Makoto Uchiyama[1,2], Kayoko Yokoi[1], Toshiyuki Ishioka[3], Yoshiyuki Hosokai[4], Kazumi Hirayama[1,5], Hiroshi Fukuda[6], Masashi Aoki[7], Takafumi Hasegawa[7], Atsushi Takeda[8], Etsuro Mori[1]

1 Department of Behavioral Neurology and Cognitive Neuroscience, Tohoku University School of Medicine, Sendai, Japan, **2** Department of Speech, Language and Hearing Sciences, Niigata University of Health and Welfare, Niigata, Japan, **3** Department of Occupational Therapy, Saitama Prefectural University, Koshigaya, Japan, **4** Department of Diagnostic Image Analysis, Tohoku University School of Medicine, Sendai, Japan, **5** Department of Occupational Therapy, Yamagata Prefectural University of Health Science, Yamagata, Japan, **6** Department of Radiology and Nuclear Medicine, Institute of Development, Aging, and Cancer, Tohoku University, Sendai, Japan, **7** Department of Neurology, Tohoku University School of Medicine, Sendai, Japan, **8** Department of Neurology, Sendai Nishitaga Hospital, Sendai, Japan

Abstract

Background: The neuropsychological features and neuropathological progression patterns associated with rapidly evolving cognitive decline or dementia in Parkinson's disease (PD) remain to be elucidated.

Methods: Fifty-three PD patients without dementia were recruited to participate in a 3-year longitudinal cohort study. The patients were grouped according to the Clinical Dementia Rating (CDR). Group-wise comparisons were made with regard to demographic characteristics, motor symptoms, neuropsychological performances and 18F-fluorodeoxyglucose positron emission tomography.

Results: Patients who had memory-plus cognitive impairment (patients whose CDR was 0 at baseline and 0.5 in memory and other domains at follow-up, and those whose baseline CDR was 0.5 in memory and other domains) exhibited higher age at onset, visuoperceptual impairment, non-tremor-dominant motor disturbance, rapid symptomatic progression and posterior neocortical hypometabolism. In patients who were cognitively unimpaired and those who had memory-dominant cognitive impairment (patients whose CDR was 0 at baseline and 0.5 only in memory domain at follow-up, and those whose baseline CDR was 0.5 only in memory domain), the posterior neocortex was relatively unaffected until a later stage of the disease.

Conclusions: These results suggest that visuoperceptual impairment and the early involvement of the posterior neocortex may be risk factors for rapid symptomatic progression and dementia in PD.

Citation: Shoji Y, Nishio Y, Baba T, Uchiyama M, Yokoi K, et al. (2014) Neural Substrates of Cognitive Subtypes in Parkinson's Disease: A 3-Year Longitudinal Study. PLoS ONE 9(10): e110547. doi:10.1371/journal.pone.0110547

Editor: Stephen D. Ginsberg, Nathan Kline Institute and New York University School of Medicine, United States of America

Received July 7, 2014; **Accepted** September 15, 2014; **Published** October 20, 2014

Data Availability: The authors confirm that all data underlying the findings are fully available without restriction. All relevant data are within the paper.

Funding: This work was supported by a Grant-in-Aid for Scientific Research (B) (24390278 to EM) and a Grant-in-Aid for Scientific Research for Young Scientists (90451591 to YN). The funders had no role in study design, data collection and analysis, decision to publish, or preparation of the manuscript.

Competing Interests: The authors have declared that no competing interests exist.

* Email: nishiou@med.tohoku.ac.jp

Introduction

The cognitive features of Parkinson's disease (PD) are heterogeneous and can be categorized into several major subtypes. [1,2] However, the neural substrates underlying the cognitive subtypes remain to be elucidated. Recent studies have demonstrated that there are correlations between cognitive impairment and non-cognitive features in PD: patients who develop dementia have a higher age of onset, rapid symptomatic progression, anosmia and a non-tremor-dominant motor subtype. [3,4,5,6] Consistent with these observations, neuropathological studies have suggested that the anatomical distribution of Lewy-related pathology differs depending on the clinical subtypes. The pathology rapidly evolves from the brainstem into the cerebral cortex in patients with the non-tremor-dominant motor subtype and/or dementia, whereas it is relatively confined to the brainstem for a longer period of time in patients with a tremor-dominant motor subtype and no cognitive impairment. [7] If such provisional clinico-pathological relationships are genuine and if specific subtypes of cognitive impairment are associated with the future development of dementia, these cognitive subtypes may be associated with specific clinico-pathological subtypes.

Previous morphometric MRI and 18F-fluorodeoxyglucose positron emission tomography (FDG-PET) studies have demonstrated greater frontal, temporal and occipital gray matter volume reduction and greater frontal and parietal cortical hypometabolism in PD patients with dementia or mild cognitive impairment (MCI) compared with cognitively unimpaired patients. [8,9,10,11,12] In agreement with these neuroimaging findings, several neuropathological studies demonstrated the relationship

between dementia and limbic and/or neocortical neurodgeneration. [13,14,15] However, there is only a little evidence for neuroimaging features predictive of later development of dementia and for distinctive progression patterns of cortical lesions among the PD subtypes. The sole previous longitudinal FDG-PET study of PD demonstrated that patients who developed dementia 1 to 3 years later exhibited occipito-parietal hypometabolism at baseline. [16] To further address this issue, we investigated the relationship among cognitive subtypes, other clinical features and changes in regional brain glucose metabolism (CMRglc) over 3 years in a cohort of PD patients.

Methods

All procedures in this study followed the clinical study guidelines of Tohoku University Hospital and were approved by its ethics committee. The patients gave written informed consent after receiving a detailed explanation of the study. When the patients had a compromised ability to consent, their family members gave consent on behalf of the patients.

Subjects

We analyzed 55 patients with PD without dementia (mean age 65.4±6.5 years; 27 women) who participated in a 3-year longitudinal study at Tohoku University Hospital. Details of the study design have been described elsewhere. [3,9,17] Briefly, outpatients at the movement disorder clinic who met the following criteria were recruited in the study: fulfillment of the diagnostic criteria of the United Kingdom Parkinson's Disease Society Brain Bank; aged 50 years or more; absence of dementia according to the Diagnostic Statistical Manual-IIIR [18] and a Clinical Dementia Rating (CDR) [19] overall score of 0 or 0.5, no evidence of diabetes mellitus; no history of other neurological or psychiatric diseases; and no evidence of infarcts, bleedings, tumors and other focal brain lesions on MRI. Of 88 consecutive patients, 33 patients dropped out for the following reasons: 4 patients died; 4 were institutionalized; 1 developed psychosis; 2 developed myocardial infarction or cerebral infarction; 9 moved to hospitals near their homes; 6 did not return for follow-up visits for unknown reasons; the initial diagnosis of PD was dismissed in 3 patients; and 4 were excluded because of incomplete clinical or imaging data. Fourteen healthy volunteers (mean age 63.1±4.4 years; 6 women) were recruited as controls for neuroimaging. There were no significant differences in age ($t = 1.6$, $p = 0.1$) or sex ($x^2 = 0.2$, $p = 0.7$) between the patient and control groups.

Comparison of patient classification procedures: the neuropsychology-based criteria versus the Clinical Dementia Rating

Measuring cognitive changes is challenging because there is no very reliable change measures. Practice effects associated with the repeated administration have a great impact on neuropsychological test performance, yielding spurious cognitive improvement over time. [20,21,22,23] A recent study demonstrated that previous test exposures lead to bias towards normal cognition in the diagnosis of MCI. [24]In addition, cognitive assessment in PD is complicated by motor symptoms, such as bradykinesia and tremor, and medication-related effects. [2] To take these problems into account, global cognitive measures and/or caregiver interviews have been used in longitudinal intervention trials for cognitive disorders. [25,26,27,28] According to this convention, we have introduced the CDR, a global cognitive measure based on examinations by clinicians and caregiver interview, in our cohort study of PD. [3,9,17] To examine the rationality of the use of the CDR in the classification of cognitive status in PD, we compared the 3-year cognitive changes based on the neuropsychology-based criteria for MCI in PD (PD-MCI) and those based on the CDR in the patients ($n = 46$) who completed neuropsychological tests for memory, visuoperceptual ability and attention/working memory (see below for the details of the neuropsychological tests). PD-MCI was defined according to the Movement Disorder Society Guideline for PD-MCI Level I (MDS PD-MCI criteria), in which the diagnosis of PD-MCI required impairments of 1 to 2 standard deviations (SDs) below norms on at least 2 neuropsychological tests. [29] In the CDR-based criteria, the patients were classified as CDR 0 (unimpaired cognition) or CDR 0.5 (cognitive impairment which mildly affecting their everyday life).

Patient classification based on the Clinical Dementia Rating

The CDR, which was designed to provide a rating scale for subjects from normal cognition through various stages of dementia, is widely considered to be a reliable scale for staging the severity of cognitive dysfunction. [19] The CDR comprises 6 subdomains, i.e., memory, orientation, judgment and problem solving, community affairs, home and hobbies and personal care. In matters related to the domains of community affairs, home and hobbies, and personal care, we asked the patients and their caregivers about cognition-related functional decline separately from disability arising from physical impairment in order to eliminate as far as possible the effects of non-cognitive symptoms. [9,17].

The primary aim of the current study is to discover clinical features and distinctive brain metabolic patterns of patients who have rapid cognitive deterioration. To this end, we first focused on 40 patients who were cognitively unimpaired (CDR 0) at baseline. Among these patients, 26 patients were cognitively unchanged over 3 years (CDR 0 at the third year; non-converters), 7 worsened only in the memory domain (memory-only converters) and 6 worsened in the memory and non-memory domains (memory-plus converters). The remaining patient, who showed deterioration only in a non-memory domain, was excluded from the analyses. Second, we analyzed patients whose overall CDR scores were 0.5 at baseline to investigate longitudinal brain metabolic changes after PD patients developed mild cognitive deficits. Eight patients who scored ≥0.5 only in the memory domain at baseline (baseline memory-only) and 6 patients who scored ≥0.5 in the memory and other domains (baseline memory-plus) were recruited for the study. We speculated that the baseline memory-only and the baseline memory-plus patients may represent the clinico-pathological stages following the memory-only converters and the memory-plus converters, respectively. We conducted group comparisons separately among the groups of baseline CDR 0, specifically non-converter, memory-only converter and memory-plus converter patients, and between the groups of baseline CDR 0.5, specifically baseline memory-only and baseline memory-plus patients, because our interest was in longitudinal changes in clinical symptoms and brain glucose metabolism.

Cognitive and motor assessments

The Mini-Mental State Examination (MMSE) and the Word Recall subtest of the Alzheimer's Disease Assessment Scale (ADAS) were used to assess general cognitive function and episodic memory, respectively. [30,31] Visuoperception was assessed using the correct response score on the overlapping-figure identification test. [32] A subset of patients underwent the backwards digit-span test to assess their working memory (the number of patients is indicated in **Tables 1 and 2**). [29] Further

details have been described elsewhere. [17,32] Motor symptoms were assessed using the Unified Parkinson's Disease Rating Scale (UPDRS) part III. We calculated the rate of progression indices for the clinical measures described above using the following formula: (rate of progression) = [(third year score)-(baseline score)]/(years of interval). [33] The tremor and non-tremor motor scores were calculated based on the UPDRS parts II and III. [5].

Statistical analyses

Group-wise comparisons of demographic data and baseline scores and progression rates of the cognitive and motor measures were analyzed using the statistical methods described in the captions of **Tables 1 and 2**. Two-way repeated-measures analysis of variance (ANOVA) with motor subtypes (the tremor and non-tremor scores of UPDRS) and time (baseline and third year) was performed to characterize the motor features of the groups. To enable comparisons with previous studies in which cognitive subtypes were determined by neuropsychological test scores, we investigated the number of patients whose scores were 1 SD or more below the mean of normative data for the ADAS-word recall, overlapping figure and backwards digit-span tests.

18F-fluorodeoxyglucose positron emission tomography

The mean interval between the clinical assessments and the positron emission tomography (PET) scan was 4.6 days. Each patient had fasted, and dopaminergic medication had been discontinued for at least 5 hours before the scan. Scanning was performed after an injection of 185–218 MBq 18F-fluorodeoxyglucose (FDG). After an FDG-uptake period of 1 hour, a 20-minute scan was acquired while the patient was at rest. Details of the scanning procedures have described elsewhere. [17,32] Image pre-processing and statistical analysis were performed using SPM5 (http://www.fil.ion.ucl.ac.uk/spm/). All images were normalized onto the standard FDG template with nonlinear warping algorithms, reconstructed into 2 mm^3 isotropic voxels and smoothed with 10 mm full width at half-maximum. Global normalisation was performed using proportional scaling, and threshold masking was set at 0.8. Cross-sectional comparisons between the patient groups and the controls were performed using *t*-test. Two-way repeated-measures ANOVA was used for cross-sectional and longitudinal comparisons of the patient groups. Age and sex were included as nuisance variables in all of the comparisons. The UPDRS part III score was included as a nuisance variable in the comparisons among the patient groups. The statistical threshold was set at an uncorrected $p<0.001$ at the voxel level and at 20 voxels at the cluster level.

Results

Comparison between the neuropsychology-based criteria and the Clinical Dementia Rating-based criteria

The results are summarized in **Figure 1.** The neuropsychology-based classification according to the MDS PD-MCI criteria exhibited a spurious improvement over 3 years in 5 of the 12 patients who were classified to PD-MCI at baseline, whereas such an effect was observed only in 1 of the 11 patients who scored 0.5 on the baseline CDR (**Figure 1**). Based on these preliminary findings, we decided to employ the CDR-based cognitive criteria in the current study.

Clinical profiles of the patient groups of baseline Clinical Dementia Rating 0

The results are summarized in **Table 1**. There were no significant differences among the non-converters, memory-only converters and memory-plus converters in sex, education, disease duration, levodopa equivalent dose or test-retest interval. The memory-plus converters had a significantly higher age of onset and a higher age at baseline than did the non-converters.

Baseline performance of the overlapping figure test was lower in the memory-plus converters than in the non-converters ($F = 10.1$, $p<0.001$). The baseline performance of the backwards digit-span was worse in the memory-only converters than it was in the non-converters ($F = 7.1$, $p<0.01$). No group differences were observed in baseline MMSE or baseline ADAS word recall. There were no significant differences in the progression rate on any of the cognitive tests.

No significant difference was observed in the baseline UPDRS part III among the three groups. The progression rate of the UPDRS part III was greater in the memory-plus converters than it was in the non-converters and the memory-only converters ($F = 6.8$, $p<0.01$). The UPDRS non-tremor score was higher in the memory-plus converters than it was in the other groups ($F = 18.8$, $p<0.001$), and no significant main effect of time or interaction between motor subtypes and times was observed.

Clinical profiles of the patient groups of baseline Clinical Dementia Rating 0.5

The results are summarized in **Table 2**. There were no significant differences between the baseline memory-only and the baseline memory-plus patients in age at baseline, sex, education, age of onset, disease duration, levodopa equivalent dose or test-retest interval. No significant group differences were observed in the baseline scores or progression rates on any of the cognitive tests. No significant difference was observed in the baseline UPDRS part III score. The UPDRS part III progression rate was greater in the baseline memory-plus patients than it was in the baseline memory-only patients ($t = -2.4$, $p<0.05$). The UPDRS non-tremor score was higher in the baseline memory-plus patients than it was in the baseline memory-only patients ($F = 8.0$, $p< 0.001$).

Positron emission tomography: comparisons between patient groups and controls

Compared with the controls, the non-converters and memory-only converters exhibited patchy, discrete areas of hypometabolism in the frontal, temporal and occipital cortices at baseline (**Figures 2A and 2B**). The memory-plus converters showed extensive hypometabolic areas in the temporo-parietal and occipital cortices compared with the controls (**Figure 2C**).

The regional pattern of metabolic reduction relative to the controls was similar among the baseline memory-only patients, the non-converters and the memory-only converters (**Figure 2D**). The baseline memory-plus patients showed a similar but more extensive hypometabolism compared with the memory-plus converters, in whom the metabolic reduction relative to controls was greatest in the temporo-parietal and medial parietal cortices (**Figure 2E**).

Positron emission tomography: comparisons among the patient groups of baseline Clinical Dementia Rating 0

At baseline, there was no significant difference in regional glucose metabolism between the non-converters and memory-only converters (**Figure 3A**). The memory-plus converters showed a

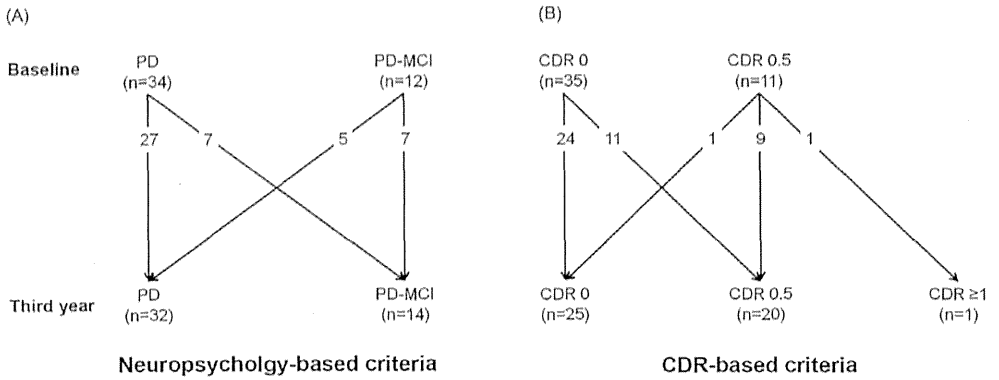

Figure 1. Diagrams of the 3-year cognitive changes observed in patients. In (A), the patients were classified as having Parkinson's disease without cognitive impairment (PD) or PD with mild cognitive impairment (PD-MCI) based on neuropsychological tests. (B) shows the results based on the Clinical Dementia Rating (CDR)-based patient classification.
doi:10.1371/journal.pone.0110547.g001

stronger metabolic reduction in the parietal and occipital cortices compared with the non-converters and amnesic converters at baseline (**Figures 3B and 3C**).

The non-converters showed a significant metabolic decline over 3 years in the frontal, temporal, medial parietal and occipital cortices and the thalamus (**Figure 4A**). In the memory-only converters, regional glucose metabolism was decreased in the anterior cingulate cortex, medial temporal lobe, caudate nucleus and midbrain over 3 years (**Figure 4B**). No significant longitudinal metabolic change was observed in the memory-plus converters (**Figure 4C**). An ANOVA interaction demonstrated that metabolic decline over 3 years in the medial temporal lobe was greater in the memory-only converters than it was in the non-converters (**Figure 4F**).

Positron emission tomography: comparisons between the patient groups of baseline Clinical Dementia Rating 0.5

The baseline memory-only patients had lower baseline regional glucose metabolism in the medial temporal lobe, cingulate cortex and dorsal brainstem regions than did the baseline memory-plus patients, whereas the regional glucose metabolism in the temporo-parietal and medial parietal cortices was lower in the baseline memory-plus patients than it was in the baseline memory-only patients (**Figures 3D and 3E**).

Regional glucose metabolism was decreased over 3 years in the parietal cortex in the baseline memory-only patients, whereas a longitudinal metabolic decline was observed in discrete regions of the basal forebrain and the brainstem in the baseline memory-plus patients (**Figures 4D and 4E**). An ANOVA interaction revealed circumscribed ventral frontal and basal forebrain regions that showed a greater 3-year metabolic decline in the baseline memory-plus patients than in the baseline memory-only patients (**Figure 4G**).

Discussion

Early visuoperceptual impairment and posterior cortical hypometabolism may represent the clinical subtypes of rapidly progressive motor symptoms and severe cognitive impairment

The clinical entity of PD encompasses a wide variety of symptoms, including motor, sensory, cognitive and autonomic disturbances. Recent cluster-analysis studies have suggested that two major clinical subtypes can be extracted from the clinical diversity: one subtype is characterized by a young age of onset, slow disease progression, tremor-dominant motor features and preserved cognition, and the other is associated with an older age of onset, rapid disease progression, non-tremor-dominant motor features and cognitive impairment. [5,6,34] In parallel with these discoveries, there has been growing evidence of the neuropathological diversities underlying these clinical subtypes. Patients with a young age of onset, slow progression and tremor-dominant motor features are reported to have neuropathological features that conform to Braak's pathological staging scheme, in which Lewy-related pathology begins in the lower brainstem (stages 1–2); ascends to the midbrain (stage 3), thalamus and limbic structures (stages 4); and finally reaches the neocortex (stages 5–6). [35] By contrast, patients with an older age of onset, non-tremor-dominant motor features and/or dementia are associated with disproportionately severe neocortical Lewy-related pathology and concomitant Alzheimer's disease-related pathology. [14,15].

In the current study, the memory-only converters showed a metabolic decline over 3 years in the anterior cingulate and medial temporal cortices (**Figure 4B**). The baseline memory-only patients, whose baseline cognitive status was similar to that of the memory-only converters at the third year, showed a metabolic decline in the parietal cortex (**Figure 4D**). Assuming that these patient groups represent a single cognitive subtype at different time points, these results suggest that neurodegeneration first affects the limbic structures and next encroaches on the posterior neocortex. This pattern of brain metabolic changes is largely consistent with Braak's scheme. [7] A longitudinal PET analysis of the non-converters demonstrated 3-year metabolic decline in the thalamus and occipital cortex (**Figure 4A**). A direct comparison between the non-converters and the memory-only converters revealed no significant group difference at baseline but greater metabolic decline over time in the memory-plus converters than in the non-converters (**Figures 3A and 4F**). These two groups of patients may represent slightly different subpopulations of a clinico-pathological subtype that conforms to Braak's scheme.

The memory-plus converters exhibited extensive posterior cortical hypometabolism at baseline compared with the controls and the non-converters (**Figures 2C, 3B and 3C**). Likewise, more extensive posterior cortical hypometabolism was observed in the baseline memory-plus patients compared with the baseline

Table 1. Demographic and clinical profiles of patients with a Clinical Dementia Rating of 0 at baseline.

		Non-converter (N = 26)	Memory-only converter (N = 7)	Memory-plus converter (N = 6)	Differences among groups
Age at baseline (years)		62.2±5.9	67.7±5.5	71.8±2.6	Memory-plus>Non-converters[b]
Gender (male/female)		12/14	2/5	1/5	
Education (years)		11.8±2.5	11.1±2.5	12.0±2.8	
Test-retest interval (days)		1140.2±110.7	1107.7±43.5	1109.7±59.7	
Disease duration at baseline (years)		4.3±3.7	5.0±6.9	5.0±3.2	
Age at onset (years)		58.0±7.3	63.6±6.0	67.2±5.4	Memory-plus>Non-converters[b]
Levodopa equivalent dose at baseline (mg/day)		303.5±233.1	378.9±320.4	533.6±340.2	
UPDRS part III	Baseline	18.0±7.3	18.9±8.0	16.5±6.2	
	Progression rate (/years)	−0.02±2.0	−0.8±0.8	4.0±5.2	Memory-plus>Non-converters[b]; Memory-plus> Memory-only[b]
UPDRS tremor score¶	Baseline	0.5±0.4	0.4±0.6	0.3±0.4	
	Third year	0.3±0.3	0.2±0.2	0.3±0.3	Main effect of non-tremor score: Memory-plus> Non-converters[b]; Memory-plus>Memory-only[b]
UPDRS non-tremor score ¶	Baseline	0.7±0.3	0.7±0.4	0.7±0.2	
	Third year	0.8±0.3	0.7±0.4	1.6±0.2	
CDR sum of boxes	Baseline	0	0	0	NE
	Third year	0	0.5	1.8±0.8	NE
MMSE	Baseline (/30)	28.2±1.8	27.3±2.6	27.5±1.9	
	Progression rate (/years)	0.1±0.6	−0.1±0.9	−0.6±0.7	
ADAS word recall†	Baseline (/30)	19.3±3.4	17.3±4.5	17.8±4.4	
	Progression rate (/years)	0.6±0.9	1.2±1.1	−0.03±1.2	
Overlapping figure‡	Baseline (/40)	33.4±4.0	29.6±2.4	25.3±6.3	Non-converters>Memory-plus[b]
	Progression rate (/years)	−0.2±1.0	0.7±0.9	−0.9±2.0	
Backward digit-span§	Baseline	4.4±0.8	3.0±0.9	4.0±0.7	Non-converters>Memory-only[a]
	Progression rate (/years)	−0.1±0.3	0.1±0.4	−0.2±0.2	
# of patients below −1 SD at baseline and at third year	ADAS word recall †	9/26 3/26	3/7 1/7	3/6 3/6	NE
	Overlapping figure‡	4/26 3/26	2/7 0/7	5/6 5/6	NE
	Backward digit-span§	1/25 5/25	4/6 4/6	1/5 3/5	NE

Analysis of variance with post-hoc Tukey's test was used for group-wise comparisons of baseline scores and progression rates except for the UPDRS tremor/non-tremor scores. Two-way analysis of variance with post-hoc Tukey's test was used for the UPDRS tremor/non-tremor scores. Data are given as the mean±SD except for the fields with asterisks. a and b indicate $p<0.05$ and $p<0.01$, respectively.

*Data are given as (the number of patients below −1 SD)/(the number of patients who underwent the test).

¶The scores were calculated according to Lewis and colleagues. [5] Data were obtained from 21 non-converters, 6 memory-only converters and 5 memory-plus converters.

†The mean score for controls (n = 20, 65.5±4.8 years) is 21.3±3.5. [49].

‡The mean score for controls (n = 24, 66.1±5.3 years) is 32.9±4.4. [32].

§The mean score for controls (n = 20, 65.5±4.8 years) is 4.8±1.0. [49].

Abbreviations: UPDRS, Unified Parkinson's Disease Rating Scale; CDR, Clinical Dementia Rating; MMSE, Mini-Mental State Examination; ADAS, Alzheimer's Disease Assessment Scale; NE, not examined.

doi:10.1371/journal.pone.0110547.t001

Table 2. Demographic and clinical profiles of patients with a Clinical Dementia Rating of 0.5 or more at baseline.

		Baseline memory-only (N = 8)		Baseline memory-plus (N = 6)		Differences between groups
Age at baseline (years)		69.0±6.6		66.2±5.5		
Gender (male/female)		6/2		6/0		
Education (years)		12.3±2.3		14.3±2.7		
Test-retest interval (days)		1115.3±107.1		1096.7±54.7		
Disease duration at baseline (years)		6.8±3.3		9.7±6.8		
Age at onset (years)		62.4±6.6		56.6±8.0		
Levodopa equivalent dose at baseline (mg/day)		453.6±163.1		658.6±337.9		
UPDRS part III	Baseline	27.1±5.4		23.8±6.6		
	Progression rate (/years)	−0.7±3.3		4.6±5.0		Baseline memory-plus>Baseline memory-only[a]
UPDRS tremor¶	Baseline	0.7±0.5		0.4±0.6		
	Third year	0.3±0.2		0.4±0.7		Main effect of non-tremor score: Baseline memory-plus> Baseline memory-only[a]
UPDRS non-tremor¶	Baseline	1.2±0.2		1.0±0.1		
	Third year	1.1±0.2		1.7±0.7		
CDR sum of boxes	Baseline	0.5		2.1±1.3		NE
	Third year	1.4±1.2		5.3±4.1		NE
MMSE	Baseline (/30)	27.0±3.0		27.0±2.2		
	Progression rate (/years)	−0.3±0.7		−1.1±2.7		
ADAS word recall†	Baseline (/30)	17.9±4.1		14.3±5.4		
	Progression rate (/years)	−0.1±1.4		−0.3±1.2		
Overlapping figure‡	Baseline (/40)	29.6±4.1		29.4±6.2		
	Progression rate (/years)	0.1±1.1		−2.4±3.1		
Backward digit-span§	Baseline	3.6±1.0		3.8±0.5		NE
	Progression rate (/years)	−0.1±0.1		−0.3±0.3		NE
# of patients below −1 SD at baseline and at third year	ADAS word recall†	4/8	3/8	5/6	5/6	NE
	Overlapping figure‡	3/8	4/8	2/5	5/5	NE
	Backward digit-span§	3/7	4/7	1/4	2/4	NE

Two-sample *t*-tests were used for group-wise comparisons of baseline scores and progression rates except for the UPDRS tremor/non-tremor scores. A two-way analysis of variance was used for the UPDRS tremor/non-tremor scores. No group-wise comparisons were performed for the backward digit-span owing to the small number of subjects. Data are given as the mean±SD except for the fields with asterisks. a and b indicate $p<0.05$ and $p<0.01$, respectively.

*Data are given as (the number of patients below −1 SD)/(the number of patients who underwent the test).

¶The scores were calculated according to Lewis and colleagues. [5] Data were obtained from 6 baseline memory-only and 6 baseline memory-plus patients.

†The mean score of controls (n = 20, 65.5±4.8 years) is 21.3±3.5. [49].

‡The mean score of controls (n = 24, 66.1±5.3 years) is 32.9±4.4. [32].

§The mean score of controls (n = 20, 65.5±4.8 years) is 4.8±1.0. [49]; a statistical comparison was not performed owing to an insufficient number of subjects.

Abbreviations: UPDRS, Unified Parkinson's Disease Rating Scale; CDR, Clinical Dementia Rating; MMSE, Mini-Mental State Examination; ADAS, Alzheimer's Disease Assessment Scale; NE, not examined.

doi:10.1371/journal.pone.0110547.t002

memory-only patients (**Figures 2E and 3E**). These findings can be interpreted in two ways: the posterior neocortical hypometabolism found in these patients may represent pathological changes in Braak stages 5–6, or they may represent a pathological progression pattern that does not conform to Braak's scheme. [7] The latter was suggested by the following clinical and neuroimaging findings. First, the severity of motor symptoms at baseline was equivalent in the memory-plus converters, non-converters and memory-only converters, suggesting that the three groups had similar degrees of midbrain pathology. In other words,

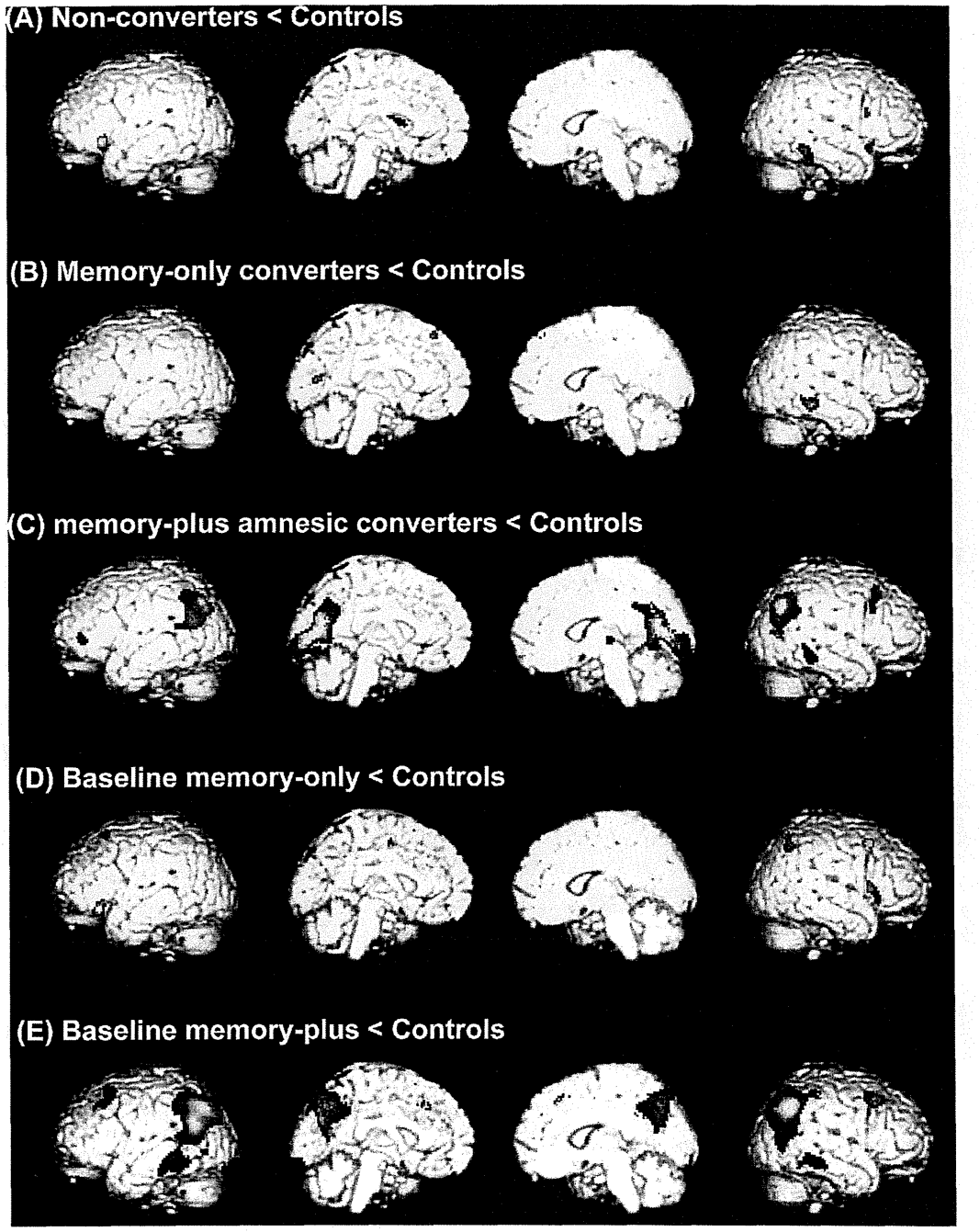

Figure 2. Areas of relative reduction in regional cerebral glucose metabolism in the patient groups compared with controls. Rendered images are shown in the order of the left lateral, left medial, right medial and right lateral.
doi:10.1371/journal.pone.0110547.g002

if the memory-plus converters represented a more advanced stage of the disease than did the other groups, they would not present with an equivalent severity of motor symptoms. Second, a comparison of metabolic patterns between the baseline memory-only and the baseline memory-plus patients showed a double dissociation in which posterior neocortical hypometabolism was more severe in the baseline memory-plus patients, whereas hypometabolism in the medial temporal lobe was more severe in the baseline memory-only patients (**Figures 3D and 3E**). These findings suggest that the brainstem and neocortex may be affected nearly simultaneously without marked limbic involvement in the memory-plus converters and the baseline memory-plus patients. A parallel finding was reported in a population-based cohort study in which incidental Lewy-related pathology was found in the

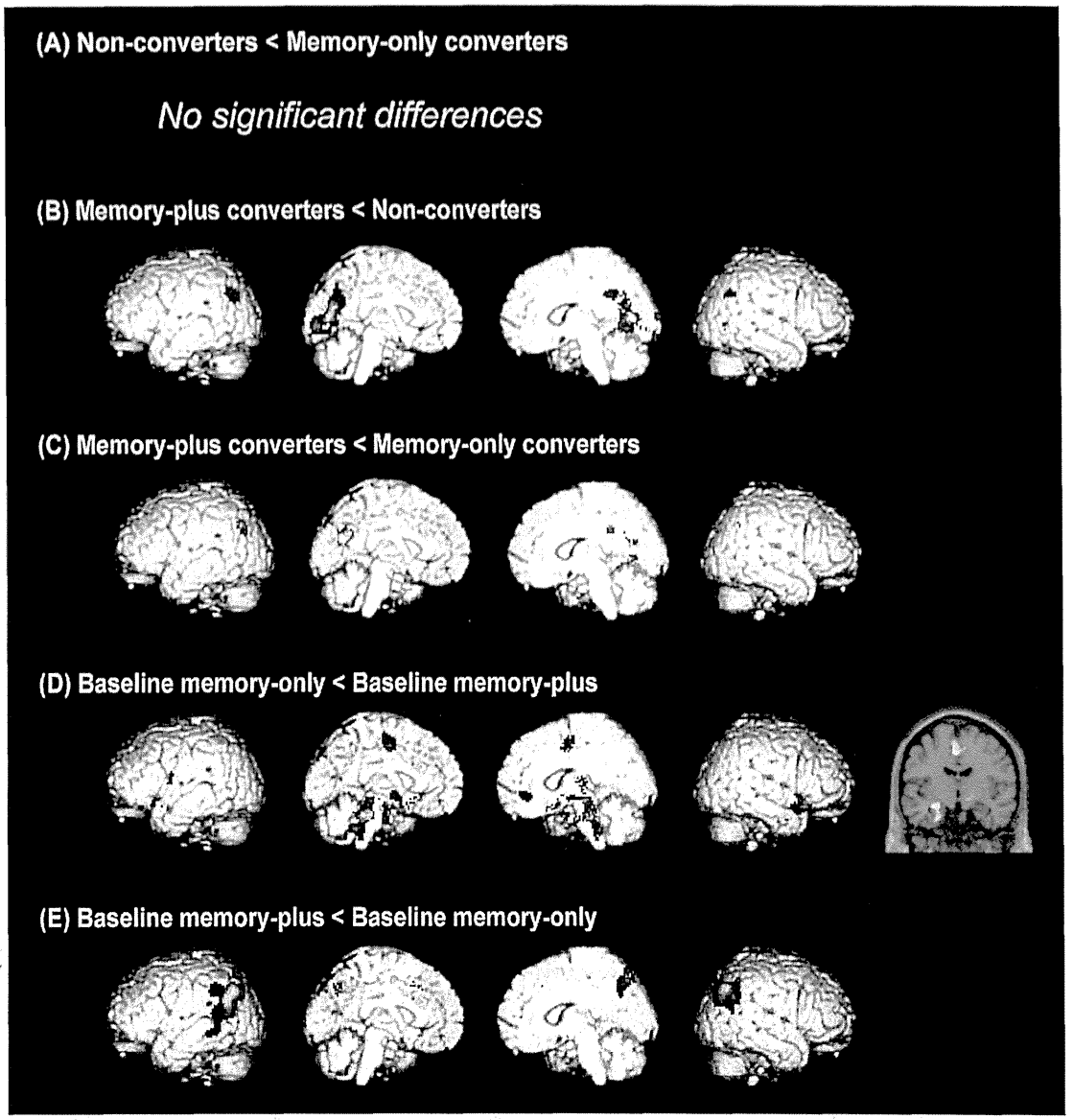

Figure 3. Group comparisons of regional cerebral glucose metabolism at baseline. (A) to (C) show the results of comparisons between patient groups with baseline Clinical Dementia Rating (CDR) 0, and (D) and (E) show the results of comparisons between groups with baseline CDR 0.5. Rendered images are shown in the order of the left lateral, left medial, right medial and right lateral. The left side of a coronal section corresponds to the left side of the brain.
doi:10.1371/journal.pone.0110547.g003

brainstem and neocortex but not in the limbic structures (medial temporal and cingulate cortices) in 3% of cases. [36].

From the viewpoint of prediction and early intervention, it is critical to establish the cognitive and neuroimaging features that are associated with rapid symptomatic deterioration and the future development of dementia. [2] In the current study, the memory-plus converters exhibited clinical features that are consistent with those of the clinical subtype associated with the rapid progression of motor symptoms and/or dementia, including rapid declines in the CDR sum of boxes and the UPDRS part III scores, and non-tremor dominant motor features (**Table 1**). [4,5,6] They had impaired performance on the overlapping-figure test (**Table 1**) and posterior cortical hypometabolism at baseline (**Figures 2C, 3B and 3C**), suggesting that early visuoperceptual impairment and posterior neocortical involvement may be risk factors for rapid symptomatic deterioration and the future development of dementia. The predictive value of visuoperceptual impairment for the future development of dementia in PD has been demonstrated in 3 of the 4 previous longitudinal neuropsychological studies with a follow-up of 2 years or more. [37,38,39,40] Similarly, a recent study demonstrated that patients with non-amnestic multi-domain MCI that had visuoperceptual deficits were associated with bradykinesia and gait disturbance (non-tremor-dominant motor features), suggesting a link to the rapidly progressive, dementia-

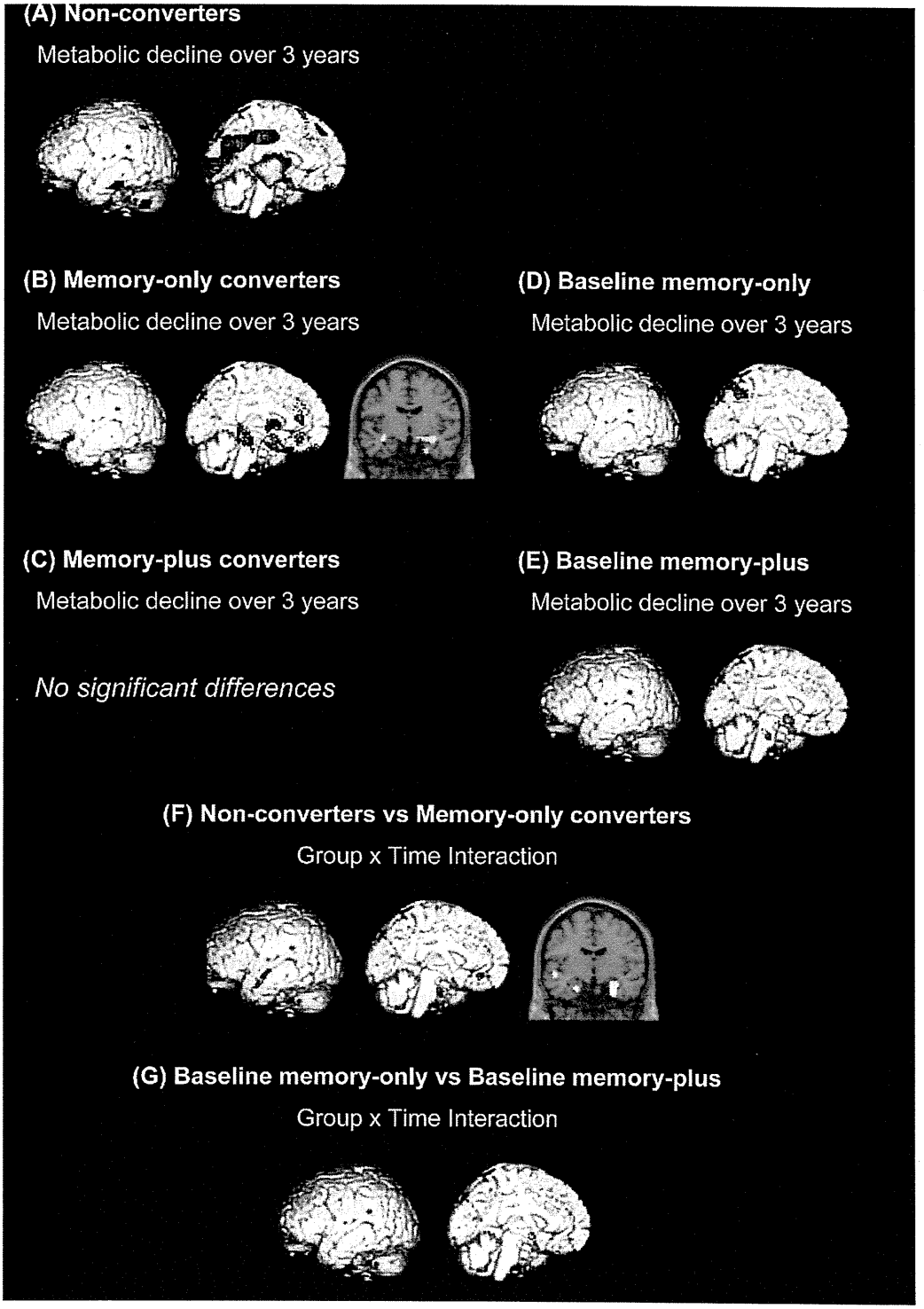

Figure 4. Longitudinal changes in regional cerebral glucose metabolism. (A) to (E) show 3-year metabolic declines in the individual patient groups. (F) and (G) show group x time interactions between the non-converters and the memory-only converters and between the baseline memory-only patients and the baseline memory-plus patients, respectively. Rendered images show the left hemisphere. The left sides of coronal sections correspond to the left side of the brain.
doi:10.1371/journal.pone.0110547.g004

related clinico-pathological subtype. [41] Although there is no neuropathological evidence for the relationship between lesions in the particular cortical regions and rapid symptomatic progression and dementia in PD, a previous longitudinal FDG-PET study demonstrated that parieto-occipital hypometabolism preceded the development of dementia. [42].

Memory impairment and its predictive value for future development of dementia in PD

Recent studies have demonstrated that memory impairment is the most common cognitive deficit in non-demented PD. [43,44] In agreement with these findings, positive scores on the memory subdomain were the most commonly observed CDR findings and baseline impairment in the ADAS-word recall test was found in 45% of the patients in the current study (**Tables 1 and 2**). However, the results of the previous longitudinal neuropsychological studies were split regarding the predictive value of memory impairment for dementia in PD. [37,38,39,40] One of the possible factors associated with this inconsistency is the variability of memory tests. The materials to be remembered (words, stories or figures) and the duration of retention (immediate or delayed) vary from test to test. Another possible factor which contribute to the low predictive value of memory impairment for dementia is the variability of the neural substrates of memory impairment in PD. Memory impairment in PD is associated with both dysexecutive retrieval deficits due to fronto-striatal dopaminergic insufficiency and mnemonic dysfunction due to hippocampal degeneration. [45] In the current study, baseline impairment on the backward digit-span observed in the memory-only converters suggests the possible contribution of executive/working memory deficits to memory complaints in PD (**Table 1**), whereas the relative medial temporal hypometabolism in the memory-only converters and the baseline memory-only patients suggested the role for hippocampal/medial temporal dysfunction (**Figures 3D, 4B and 4F**). Furthermore, a third mechanism of memory impairment is indicated by the findings of the current study; the memory-plus converters and the baseline memory-plus patients did not show significant hypometabolism in the medial temporal lobe despite their obvious memory problems, but they instead showed temporo-parietal and medial parietal hypometabolism (**Figures 2C, 2E, 3B, 3C and 3E**). The involvement of the parietal lobe in memory tasks has been documented in functional neuroimaging studies, but its functional role has been a matter of debate. [46].

Limitations

There are a number of limitations in the current study. First, although we claim that the memory-plus converters represent the rapidly progressive clinical subtype, no significant metabolic changes over 3 years were observed in this patient group. The following reasons can be suggested for this negative finding: (1) the small sample size may have result in a low statistical power; and (2) diffuse metabolic decline across the entire cerebral cortex may have obscured by the proportional scaling in the PET analysis. Consistent with the latter, a supplementary PET analysis in which a cerebellar reference was used instead of the proportional scaling demonstrated a CMRglc reduction over 3 years in the prefontal cortex in the memory-plus converters (**Figure S1**).

Second, there were substantial inconsistencies between the CDR-based criteria and performance on the individual neuropsychological tests. Although patients with a CDR of 0 were defined as cognitively normal' according to our criteria, some were impaired in one or more neuropsychological tests. This inconsistency is most likely due to the insensitivity of the CDR to slight cognitive impairment, particularly in the executive and visuoperceptual domains. By contrast, neuropsychological tests failed to detect cognitive declines over time in the memory-only converters and memory-plus converters, despite the obvious cognitive deterioration documented by the CDR (**Table 1**). Measuring longitudinal cognitive changes using neuropsychological tests is contaminated by spurious improvement associated with practice effects. [20,21,22,23] Although the neuropsychological tests were administered twice with a relatively long interval of 3 years in the current study, previous studies demonstrated that practice effects persist over 5 years and are strongest between the first and second administrations. [20,47,48] Furthermore, the impact of dopaminergic therapy on cognition and mood should be taken into account in PD patients. A formal definitions of clinically meaningful cognitive decline' in PD should be established in future studies. [29] In addition, the criteria for at-risk state for dementia or PD-MCI should be not only sensitive but also specific. Insensitive criteria would lead to the oversight of at-risk patients of dementia, whereas an overly sensitive and insufficiently specific ones would make every PD patient an at-risk one because almost every PD patient is impaired in some of highly-demanded cognitive tasks.

Third, we separately analyzed the patient groups with a baseline CDR of 0 and those with a CDR of 0.5 and integrated the results obtained from these separate analyses to discuss long-term (more than 3 years) cognitive changes. Our findings and discussion should be examined by studies with longer follow-up periods.

Finally, the reduction in glucose metabolism may reflect not only neurodegeneration itself but also the remote effects of lesions in distant neural structures. In addition, because FDG-PET is unable to differentiate between Alzheimer's disease-related and Lewy-related pathologies, further studies utilizing amyloid-PET and other neuroimaging techniques are necessary to examine these issues.

Supporting Information

Figure S1 The results of a cerebellar-referenced PET analysis for the patient groups with baseline CDR 0 (non-converters, memory-only converters and memory-plus converters). A two-way repeated-measures ANOVA with variables of no interest of age, sex and UPDRS part III score was used. The statistical threshold was set at an uncorrected $p<0.001$ at the voxel level and at 20 voxels at the cluster level.
(TIF)

Author Contributions

Conceived and designed the experiments: YS YN TB EM. Performed the experiments: YN TB MU KY TI YH KH AT. Analyzed the data: YS YN. Contributed reagents/materials/analysis tools: HF MA TH EM. Contributed to the writing of the manuscript: YS YN.

References

1. Kehagia AA, Barker RA, Robbins TW (2010) Neuropsychological and clinical heterogeneity of cognitive impairment and dementia in patients with Parkinson's disease. Lancet Neurol 9: 1200–1213.

2. Litvan I, Aarsland D, Adler CH, Goldman JG, Kulisevsky J, et al. (2011) MDS Task Force on mild cognitive impairment in Parkinson's disease: critical review of PD-MCI. Mov Disord 26: 1814–1824.

3. Baba T, Kikuchi A, Hirayama K, Nishio Y, Hosokai Y, et al. (2012) Severe olfactory dysfunction is a prodromal symptom of dementia associated with Parkinson's disease: a 3 year longitudinal study. Brain 135: 161–169.
4. Burn DJ, Rowan EN, Allan LM, Molloy S, O'Brien JT, et al. (2006) Motor subtype and cognitive decline in Parkinson's disease, Parkinson's disease with dementia, and dementia with Lewy bodies. J Neurol Neurosurg Psychiatry 77: 585–589.
5. Lewis SJ, Foltynie T, Blackwell AD, Robbins TW, Owen AM, et al. (2005) Heterogeneity of Parkinson's disease in the early clinical stages using a data driven approach. J Neurol Neurosurg Psychiatry 76: 343–348.
6. van Rooden SM, Colas F, Martinez-Martin P, Visser M, Verbaan D, et al. (2011) Clinical subtypes of Parkinson's disease. Mov Disord 26: 51–58.
7. Halliday GM, Holton JL, Revesz T, Dickson DW (2011) Neuropathology underlying clinical variability in patients with synucleinopathies. Acta Neuropathol 122: 187–204.
8. Burton EJ, McKeith IG, Burn DJ, Williams ED, O'Brien JT (2004) Cerebral atrophy in Parkinson's disease with and without dementia: a comparison with Alzheimer's disease, dementia with Lewy bodies and controls. Brain 127: 791–800.
9. Hosokai Y, Nishio Y, Hirayama K, Takeda A, Ishioka T, et al. (2009) Distinct patterns of regional cerebral glucose metabolism in Parkinson's disease with and without mild cognitive impairment. Mov Disord 24: 854–862.
10. Huang C, Mattis P, Tang C, Perrine K, Carbon M, et al. (2007) Metabolic brain networks associated with cognitive function in Parkinson's disease. Neuroimage 34: 714–723.
11. Nagano-Saito A, Washimi Y, Arahata Y, Kachi T, Lerch JP, et al. (2005) Cerebral atrophy and its relation to cognitive impairment in Parkinson disease. Neurology 64: 224–229.
12. Summerfield C, Junque C, Tolosa E, Salgado-Pineda P, Gomez-Anson B, et al. (2005) Structural brain changes in Parkinson disease with dementia: a voxel-based morphometry study. Arch Neurol 62: 281–285.
13. Aarsland D, Perry R, Brown A, Larsen JP, Ballard C (2005) Neuropathology of dementia in Parkinson's disease: a prospective, community-based study. Ann Neurol 58: 773–776.
14. Compta Y, Parkkinen L, O'Sullivan SS, Vandrovcova J, Holton JL, et al. (2011) Lewy- and Alzheimer-type pathologies in Parkinson's disease dementia: which is more important? Brain 134: 1493–1505.
15. Selikhova M, Williams DR, Kempster PA, Holton JL, Revesz T, et al. (2009) A clinico-pathological study of subtypes in Parkinson's disease. Brain 132: 2947–2957.
16. Bohnen NI, Muller ML (2013) In vivo neurochemical imaging of olfactory dysfunction in Parkinson's disease. J Neural Transm 120: 571–576.
17. Nishio Y, Hirayama K, Takeda A, Hosokai Y, Ishioka T, et al. (2010) Corticolimbic gray matter loss in Parkinson's disease without dementia. Eur J Neurol 17: 1090–1097.
18. Amrerical Psychiatric Association. (1987) Diagnostic and Statistical Manual of Mental Disorders. 3rd, revised.
19. Morris JC (1997) Clinical dementia rating: a reliable and valid diagnostic and staging measure for dementia of the Alzheimer type. Int Psychogeriatr 9 Suppl 1: 173–176; discussion 177–178.
20. Abner EL, Dennis BC, Mathews MJ, Mendiondo MS, Caban-Holt A, et al. (2012) Practice effects in a longitudinal, multi-center Alzheimer's disease prevention clinical trial. Trials 13: 217.
21. Duff K, Beglinger LJ, Schultz SK, Moser DJ, McCaffrey RJ, et al. (2007) Practice effects in the prediction of long-term cognitive outcome in three patient samples: a novel prognostic index. Arch Clin Neuropsychol 22: 15–24.
22. Machulda MM, Pankratz VS, Christianson TJ, Ivnik RJ, Mielke MM, et al. (2013) Practice Effects and Longitudinal Cognitive Change in Normal Aging vs. Incident Mild Cognitive Impairment and Dementia in The Mayo Clinic Study of Aging. Clin Neuropsychol 27: 1247–1264.
23. Mathews M, Abner E, Caban-Holt A, Kryscio R, Schmitt F (2013) CERAD practice effects and attrition bias in a dementia prevention trial. Int Psychogeriatr 25: 1115–1123.
24. Mathews M, Abner E, Kryscio R, Jicha G, Cooper G, et al. (2014) Diagnostic accuracy and practice effects in the National Alzheimer's Coordinating Center Uniform Data Set neuropsychological battery. Alzheimers Dement. doi: 10.1016/j.jalz.2013.11.007.
25. Doody RS, Ferris SH, Salloway S, Sun Y, Goldman R, et al. (2009) Donepezil treatment of patients with MCI: a 48-week randomized, placebo-controlled trial. Neurology 72: 1555–1561.
26. Dubois B, Tolosa E, Katzenschlager R, Emre M, Lees AJ, et al. (2012) Donepezil in Parkinson's disease dementia: a randomized, double-blind efficacy and safety study. Mov Disord 27: 1230–1238.
27. Mori E, Ikeda M, Kosaka K (2012) Donepezil for dementia with Lewy bodies: a randomized, placebo-controlled trial. Ann Neurol 72: 41–52.
28. Rogers SL (1998) Perspectives in the management of Alzheimer's disease: clinical profile of donepezil. Dement Geriatr Cogn Disord 9 Suppl 3: 29–42.
29. Litvan I, Goldman JG, Troster AI, Schmand BA, Weintraub D, et al. (2012) Diagnostic criteria for mild cognitive impairment in Parkinson's disease: Movement Disorder Society Task Force guidelines. Mov Disord 27: 349–356.
30. Folstein MF, Robins LN, Helzer JE (1983) The Mini-Mental State Examination. Arch Gen Psychiatry 40: 812.
31. Mohs RC, Rosen WG, Davis KL (1983) The Alzheimer's disease assessment scale: an instrument for assessing treatment efficacy. Psychopharmacol Bull 19: 448–450.
32. Ishioka T, Hirayama K, Hosokai Y, Takeda A, Suzuki K, et al. (2011) Illusory misidentifications and cortical hypometabolism in Parkinson's disease. Mov Disord 26: 837–843.
33. Schrag A, Dodel R, Spottke A, Bornschein B, Siebert U, et al. (2007) Rate of clinical progression in Parkinson's disease. A prospective study. Mov Disord 22: 938–945.
34. Reijnders JS, Ehrt U, Lousberg R, Aarsland D, Leentjens AF (2009) The association between motor subtypes and psychopathology in Parkinson's disease. Parkinsonism Relat Disord 15: 379–382.
35. Braak H, Del Tredici K, Rub U, de Vos RA, Jansen Steur EN, et al. (2003) Staging of brain pathology related to sporadic Parkinson's disease. Neurobiol Aging 24: 197–211.
36. Zaccai J, Brayne C, McKeith I, Matthews F, Ince PG (2008) Patterns and stages of alpha-synucleinopathy: Relevance in a population-based cohort. Neurology 70: 1042–1048.
37. Janvin CC, Larsen JP, Aarsland D, Hugdahl K (2006) Subtypes of mild cognitive impairment in Parkinson's disease: progression to dementia. Mov Disord 21: 1343–1349.
38. Levy G, Jacobs DM, Tang MX, Cote LJ, Louis ED, et al. (2002) Memory and executive function impairment predict dementia in Parkinson's disease. Mov Disord 17: 1221–1226.
39. Mahieux F, Fenelon G, Flahault A, Manifacier MJ, Michelet D, et al. (1998) Neuropsychological prediction of dementia in Parkinson's disease. J Neurol Neurosurg Psychiatry 64: 178–183.
40. Williams-Gray CH, Foltynie T, Brayne CE, Robbins TW, Barker RA (2007) Evolution of cognitive dysfunction in an incident Parkinson's disease cohort. Brain 130: 1787–1798.
41. Goldman JG, Weis H, Stebbins G, Bernard B, Goetz CG (2012) Clinical differences among mild cognitive impairment subtypes in Parkinson's disease. Mov Disord 27: 1129–1136.
42. Bohnen NI, Koeppe RA, Minoshima S, Giordani B, Albin RL, et al. (2011) Cerebral glucose metabolic features of Parkinson disease and incident dementia: longitudinal study. J Nucl Med 52: 848–855.
43. Aarsland D, Bronnick K, Williams-Gray C, Weintraub D, Marder K, et al. (2010) Mild cognitive impairment in Parkinson disease: a multicenter pooled analysis. Neurology 75: 1062–1069.
44. Hanna-Pladdy B, Jones K, Cabanban R, Pahwa R, Lyons KE (2013) Predictors of mild cognitive impairment in early-stage Parkinson's disease. Dement Geriatr Cogn Dis Extra 3: 168–178.
45. Aarsland D, Bronnick K, Fladby T (2011) Mild cognitive impairment in Parkinson's disease. Curr Neurol Neurosci Rep 11: 371–378.
46. Wagner AD, Shannon BJ, Kahn I, Buckner RL (2005) Parietal lobe contributions to episodic memory retrieval. Trends Cogn Sci 9: 445–453.
47. Rabbitt P, Lunn M, Ibrahim S, McInnes L (2009) Further analyses of the effects of practice, dropout, sex, socio-economic advantage, and recruitment cohort differences during the University of Manchester longitudinal study of cognitive change in old age. Q J Exp Psychol (Hove) 62: 1859–1872.
48. Rabbitt P, Lunn M, Wong D, Cobain M (2008) Age and ability affect practice gains in longitudinal studies of cognitive change. J Gerontol B Psychol Sci Soc Sci 63: P235–P240.
49. Abe N, Fujii T, Hirayama K, Takeda A, Hosokai Y, et al. (2009) Do parkinsonian patients have trouble telling lies? The neurobiological basis of deceptive behaviour. Brain 132: 1386–1395.

Neurobiology of Disease 71 (2014) 1–13

Contents lists available at ScienceDirect

Neurobiology of Disease

journal homepage: www.elsevier.com/locate/ynbdi

VPS35 dysfunction impairs lysosomal degradation of α-synuclein and exacerbates neurotoxicity in a *Drosophila* model of Parkinson's disease

Emiko Miura [a,1], Takafumi Hasegawa [a,*,1], Masatoshi Konno [a,b,1], Mari Suzuki [b], Naoto Sugeno [a], Nobuhiro Fujikake [b], Sven Geisler [c], Mitsuaki Tabuchi [d], Ryuji Oshima [a], Akio Kikuchi [a], Toru Baba [a], Keiji Wada [b], Yoshitaka Nagai [b], Atsushi Takeda [a,e], Masashi Aoki [a]

[a] Division of Neurology, Department of Neuroscience & Sensory Organs, Tohoku University Graduate School of Medicine, Sendai 980-8574, Japan
[b] Department of Degenerative Neurological Diseases, National Institute of Neuroscience, National Center of Neurology and Psychiatry (NCNP), Kodaira 187-8502, Japan
[c] Laboratory of Functional Neurogenetics, Department for Neurodegenerative Diseases, Hertie Institute for Clinical Brain Research, University of Tübingen, German Centre for Neurodegenerative Diseases (DZNE), 72076 Tübingen, Germany
[d] Laboratory of Applied Molecular Cell Biology, Faculty of Agriculture, Kagawa University, Kagawa 761-0795, Japan
[e] Department of Neurology, National Hospital Organization Sendai-Nishitaga Hospital, Sendai 982-8555, Japan

ARTICLE INFO

Article history:
Received 3 May 2014
Revised 7 July 2014
Accepted 28 July 2014
Available online 6 August 2014

Keywords:
Parkinson's disease
VPS35
α-Synuclein
Retromer
Cathepsin D
Lysosome
Vesicular transport

ABSTRACT

Mutations in *vacuolar protein sorting 35* (*VPS35*) have been linked to familial Parkinson's disease (PD). VPS35, a component of the retromer, mediates the retrograde transport of cargo from the endosome to the trans-Golgi network. Here we showed that retromer depletion increases the lysosomal turnover of the mannose 6-phosphate receptor, thereby affecting the trafficking of cathepsin D (CTSD), a lysosome protease involved in α-synuclein (αSYN) degradation. VPS35 knockdown perturbed the maturation step of CTSD in parallel with the accumulation of αSYN in the lysosomes. Furthermore, we found that the knockdown of *Drosophila VPS35* not only induced the accumulation of the detergent-insoluble αSYN species in the brain but also exacerbated both locomotor impairments and mild compound eye disorganization and interommatidial bristle loss in flies expressing human αSYN. These findings indicate that the retromer may play a crucial role in αSYN degradation by modulating the maturation of CTSD and might thereby contribute to the pathogenesis of the disease.

Introduction

Parkinson's disease (PD), the second most common neurodegenerative disease, is clinically characterized by a progressive increase in movement disability, impaired balance, and a variety of nonmotor symptoms (Poewe and Mahlknecht, 2009). The pathological hallmark of PD is the loss of pigmented dopaminergic neurons in the substantia nigra pars compacta and the presence of Lewy bodies, which are composed primarily of α-synuclein (αSYN) fibrils (Spillantini et al., 1997). During the assembly of αSYN fibrils, various intermediate-state oligomers are formed, and these oligomers are suspected to be the main toxic species (Wales et al., 2013). The mechanisms underlying the selective neuronal loss in PD remain elusive; however, numerous etiopathogenic hypotheses have been proposed related to oxidative stress, endoplasmic reticulum stress, mitochondrial dysfunction, ubiquitin–proteasome dysfunction, and an impaired autophagy–lysosome pathway (Dehay et al., 2013; Hasegawa et al., 2006; Singleton et al., 2013; Springer and Kahle, 2011; Sugeno et al., 2008; Tofaris, 2012). Although more than 90% of PD cases occur sporadically, the identification of several genes linked to familial PD has offered great insight into the biochemical and molecular mechanisms of the disease. Recently, a missense mutation (p.D620N) in the *vacuolar protein sorting 35* (*VPS35*) gene was identified as the cause of an autosomal dominant form of PD (Vilarino-Guell et al., 2011; Zimprich et al., 2011). VPS35, a vital element of the retromer complex, mediates the retrograde

Abbreviations: Ab, antibody; AD, Alzheimer's disease; αSYN, α-synuclein; CTSD, cathepsin D; CI-MPR, cation-independent mannose 6-phosphate receptor; DMEM, Dulbecco's modified Eagle's medium; elav, embryonic lethal abnormal vision; FBS, fetal bovine serum; GMR, glass multiple reporter; HMW, high-molecular-weight; HRP, horseradish peroxidase; HSP, heat shock protein; LAMP, lysosome-associated membrane protein; M6P, mannose 6-phosphate; MTT, 3-(4,5-dimethylthiazo-2-yl)-2,5-diphenyltetrazolium bromide; NAB, N-aryl benzimidazole; Nedd4, neural precursor cell expressed developmentally down-regulated protein 4; PD, Parkinson's disease; PVDF, polyvinylidene difluoride; RFU, relative fluorescence unit; RIPA, radio-immunoprecipitation assay; RNAi, RNA interference; rp49, ribosomal protein 49; siRNA, small interfering RNA; SDS, sodium dodecyl sulfate; SNX, sorting nexin; TCA, trichloroacetic acid; Tg, transgenic; TGN, trans-Golgi network; UAS, upstream activating sequence; VPS35, vacuolar protein sorting 35; WASH, Wiskott–Aldrich syndrome protein and SCAR homolog; wt, wild-type.

* Corresponding author at: Division of Neurology, Department of Neuroscience & Sensory Organs, Tohoku University Graduate School of Medicine, 1-1, Seiryomachi, Aobaku, Sendai, Miyagi 980-8574, Japan. Fax: +81 22 717 7192.
E-mail address: thasegawa@med.tohoku.ac.jp (T. Hasegawa).
Available online on ScienceDirect (www.sciencedirect.com).
[1] These authors contributed equally to this study.

http://dx.doi.org/10.1016/j.nbd.2014.07.014
0969-9961/

transport of cargo from the endosome to the *trans*-Golgi network (TGN) (Seaman et al., 1997). Structurally, the retromer comprises two distinct subcomplexes: a cargo-recognition VPS26–VPS29–VPS35 heterotrimer and a membrane-targeting dimer of the sorting nexin (SNX1 and/or SNX2) (Hierro et al., 2007). One of the best-characterized types of cargo for the retromer is the cation-independent mannose 6-phosphate receptor (CI-MPR), which participates in the delivery of lysosomal enzymes, such as the aspartyl protease cathepsin D (CTSD), to lysosomes (Seaman, 2004). Upon arrival in the Golgi apparatus, newly synthesized lysosomal enzymes are specifically modified with mannose 6-phosphate (M6P) residues, which are recognized by the CI-MPR in the TGN. Under physiological conditions, newly synthesized CTSD binds CI-MPR in the TGN and is translocated into endosomes; the CTSD is then released for further transport to lysosomes. The retromer retrieves the unoccupied MPRs from endosomes and relocates them to the TGN, where they participate in further cycles of CTSD sorting. Because CTSD is the main lysosomal endopeptidase responsible for the degradation of long-lived proteins, including αSYN (Cullen et al., 2009; Sevlever et al., 2008), it is tempting to speculate that a VPS35 malfunction may decrease the active form of CTSD in lysosomes and thus lead to an abnormal αSYN accumulation.

To further clarify the pathophysiological roles of the retromer in αSYN catabolism, RNA interference (RNAi)-mediated silencing of *VPS35* was performed using cellular and *in vivo* human wild-type (wt) αSYN (*h[wt]-SNCA*)-expressing transgenic fly models. In this study, we found that interference with the retromer function resulted in the aberrant maturation of CTSD, which led to the accumulation of intracellular αSYN, mainly in the late endosome/lysosome compartments. Furthermore, we showed that the knockdown of *Drosophila melanogaster VPS35* (*dVPS35*) exacerbated the locomotor abnormalities and mild compound eye disorganization and interommatidial bristle loss in human αSYN transgenic (Tg) flies. Our study provides evidence that the retromer may play a critical role in αSYN catabolism and thus drive the pathogenic process in synucleinopathies.

Materials and methods

Cell culture and plasmid transfection

HEK293 cells were maintained in Dulbecco's modified Eagle's medium (DMEM) with high glucose (4500 mg/L; Life Technologies/GIBCO, Carlsbad, CA) supplemented with L-glutamine and 10% fetal bovine serum (FBS; Thermo Scientific/HyClone, Rockford, IL). Plasmids (5 μg DNA for 1×10^6 cells) were introduced into these cells using the NEPA21® square wave electroporator according to the manufacturer's protocol (NEPA Gene, Chiba, Japan). Electroporation parameters consisted of a poring pulse (115 V, 7.5 ms in length with 50 ms interval) and a transfer pulse (20 V, 50 ms in length with 50 ms interval). For the stable transfection of HA-tagged and untagged αSYN in HEK293 cells, transfected cells were maintained under selective pressure with 800 μg/ml of G418 (InvivoGen, San Diego, CA).

Plasmid construction and preparation

Human CTSD cDNA (NM_001909.4) was subcloned into a pCMV vector. The cDNA encoding h[wt]-SNCA (NM_000345.3) with a Kozak consensus sequence was introduced into pcDNA3.1 + and 2xHA pRc/CMV vectors (RIKEN Bioresource Center, Tsukuba, Japan). Human wt and mutant (D620N and P316S) VPS35 cDNAs (GenBank AF175265.1) were subcloned into a pcDNA6.2/N-V5 vector (Life Technologies). Plasmid DNAs were isolated and purified using the GenoPure Plasmid Maxi Kit (Roche, Indianapolis, IN). The fidelity and orientation of the expression constructs were confirmed by restriction digestion and direct nucleotide sequencing.

RNA interference

The following small interfering RNAs (siRNAs) were used to ablate the expression of human VPS35: *VPS35* siRNA#1, 5′-GCCUUCAGAGGA UGUUGUAUCUUUA-3′ and *VPS35* siRNA#2, 5′-GCAUGAGUUGUUAU GUGCUUAGUAA-3′ (Stealth™ siRNA duplex oligoribonucleotides, Life Technologies/Invitrogen). Scrambled control siRNA (sc-36869) was purchased from Santa Cruz Biotechnology (Santa Cruz, CA). HEK293 cells were transfected with the target-specific or control scrambled siRNA (2 μg siRNA for 1×10^6 cells) using a NEPA21 square wave electroporator according to the manufacturer's protocol. Electroporation parameters included a poring pulse (115 V, 7.5 ms in length with 50 ms intervals) and a transfer pulse (20 V, 50 ms in length with 50 ms intervals). Thirty-three hours after the gene silencing, the cells were harvested and subjected to further studies. To evaluate the degradation kinetics of αSYN by CTSD, human CTSD was expressed for 24 h in HEK293 cells stably expressing αSYN. The cells were then treated with cycloheximide (0.1 μg/μl, purchased from Sigma) for 24 h. Chloroquine diphosphate (Sigma; 50 μM for 5 h) was used to examine the role of lysosomal function on αSYN degradation.

Subcellular fractionation

Subcellular fractionation was performed according to methods described previously (Hasegawa et al., 2011). In brief, mechanically harvested cells (1×10^8) were resuspended in 2 ml ice-cold fractionation buffer (10 mM Tris/acetic acid pH 7.0 and 250 mM sucrose) and homogenized using 20 strokes in a 2-ml Dounce tissue grinder with a tight pestle (GPE, Bedfordshire, England). The homogenate was cleared by three successive centrifugation steps (500 ×*g* for 2 min, 1000 ×*g* for 2 min and 2000 ×*g* for 2 min). The supernatant was centrifuged at 4000 ×*g* for 2 min to pellet the plasma membrane and nuclei. The supernatant was then ultracentrifuged at 100,000 ×*g* (P50S2 swing rotor, Hitachi Koki Co., Ltd., Tokyo, Japan) for 2 min to pellet the mitochondria, endosomes, and lysosomes (fraction EL). Lysosomes were isolated from the fraction EL by a 10-min osmotic lysis using 5 times the pellet volume of distilled water. After another centrifugation step at 100,000 ×*g* for 2 min, the lysosomes remained in the supernatant, whereas the endosomes and mitochondria were in the pellet.

Protein extraction from culture medium

Protein in the medium was extracted using a trichloroacetic acid (TCA)/acetone precipitation (Hasegawa et al., 2011). In brief, the culture medium was cleared by three successive centrifugation steps (800 ×*g* for 5 min, 2000 ×*g* for 10 min, and 10,000 ×*g* for 20 min at 4 °C). The supernatant was transferred to a new tube, and an equal volume of ice-cold 20% TCA/acetone was added, followed by incubation at −20 °C for 3 h. After adding 3 volumes of acetone, the protein was allowed to precipitate overnight at −20 °C. The protein was pelleted by centrifugation at 5000 ×*g* for 60 min, dissolved in 8 M urea/5% SDS with sonication, and subjected to Western blotting.

Cathepsin D activity assay

The bioactivity of CTSD in cultured cells was measured by a fluorescence-based assay using MCA-GKPILFFRLK(DNP)-dR-NH_2 as a synthetic substrate (CTSD Activity Assay Kit; BioVision, Mountain View, CA). Fluorescence was measured at an excitation/emission = 328/460 nm using a Varioskan Flash microplate reader (Thermo Scientific, Asheville, NC). The specific enzymatic activity was calculated as the relative fluorescence unit divided by the total protein concentration (relative fluorescence unit; RFU/μg protein). Pooled data from 5 independent experiments were statistically analyzed using one-way ANOVA with a post-hoc Dunnett's test using GraphPad Prism version 6 for Mac OS X (GraphPad Software, CA).

Western immunoblot analysis

After preparing the cell lysates using radio-immunoprecipitation assay (RIPA) buffer (1% NP-40, 0.5% deoxycholate, 0.1% sodium dodecyl sulfate (SDS), 1 mM EDTA, 10 m M sodium pyrophosphate, 50 mM sodium fluoride, 1 mM sodium orthovanadate, 150 mM sodium chloride, 50 mM Tris–HCl (pH 8.0) plus 1× Cømplete protease inhibitor cocktail; Roche), the protein concentration was determined using a BCA protein assay kit (BioRad, Hercules, CA). The lysate (15 μg) was electrophoresed on SDS-PAGE gels and transferred onto polyvinylidene difluoride (PVDF) membranes using the Trans-Blot Turbo® transfer system (BioRad). For the detection of human αSYN in the fly brain, five dissected fly heads were homogenized in Triton lysis buffer (50 mM Tris–HCl (pH 7.4), 1% Triton X-100, 150 mM NaCl, 1 mM EDTA plus protease inhibitors) using a Biomasher II® tissue grinder (Nippi Inc., Tokyo, Japan). After centrifugation at 15,000 ×g for 20 min, the supernatant was collected as the Triton-soluble fraction. The remaining pellet was further dissolved into a 2× Laemmli buffer with sonication and was centrifuged at 15,000 ×g for 20 min. The supernatant was collected as the Triton-insoluble fraction. For improved detection of αSYN in fly brain, transferred PVDF membranes were soaked in 0.4% paraformaldehyde/PBS for 30 min prior to the blocking step (Lee and Kamitani, 2011). After blocking with 5% milk in Tris-buffered saline with 0.1% Tween 20, the membranes were incubated with the following antibodies (Abs): anti-VPS35 ([C3], C-term Ab, 1:2000; GeneTex, Irvine, CA), anti-CTSD (clone C-20, 1:2000; Santa Cruz), anti-CI-MPR (#5230-1, 1:20,000; Epitomics, Burlingame, CA), anti-VPS26 (ab23892, 1:4000; Abcam, Cambridge, UK), anti-VPS29 (H00051699-A01, 1:500; Abnova, Taipei, Taiwan), anti-α-tubulin (clone DM1A, 1:1000; Sigma, St. Louis, MO), anti-syn-1 (610787, 1:1000; BD Bioscience, San Jose, CA), anti-HA-tag (clone 6E2, 1:1000; CST, Danvers, MA), anti-V5-tag (R960-25, 1:1000; Invitrogen), anti-albumin (#4929, 1:4000; CST), anti-Rab5 (clone S-19, 1:2000; Santa Cruz), anti-LAMP-2 (clone H4B4, 1:1000; DSHB, Iowa City, IA) and anti-Hsp90 (SPA-846, 1:4000; Stressgen, Victoria, BC, Canada). Primary Abs were followed by incubation with HRP-conjugated secondary Abs (1:10000; Jackson ImmunoResearch Laboratories, West Grove, PA). Bands were visualized with Luminata Forte HRP Substrate (Millipore, Bedford, MA) and images were captured by an Omega Lum G™ image analyzer (Aplegen, Pleasanton, CA). Quantification of the band intensity was performed using Image J software (NIH, Bethesda, MD). Pooled data from four independent experiments were statistically analyzed by a one-way ANOVA or unpaired Student's *t*-test.

Coimmunoprecipitation

Coimmunoprecipitation was performed according to the method described previously (Hasegawa et al., 2010). In brief, 48 h post-transfection, HEK293 cells were lysed in TNE buffer containing 50 mM Tris–HCl (pH 7.4), 150 mM NaCl, 0.5% NP-40, 1 mM EDTA and 1× protease inhibitor cocktail (Roche). Lysate containing 500 μg of protein was immunoprecipitated with 3 μl of V5 Ab (Life Technologies/Invitrogen) overnight on a carousel at 4 °C. Immune complexes were allowed to bind to Protein A/G PLUS-Agarose (Santa Cruz) for 2 h at 4 °C. After washing 5 times with TNE buffer containing 0.1% NP-40, protein complexes were eluted with 2× non-reducing Laemmli buffer and subsequently analyzed by Western blotting.

Immunofluorescence confocal microscopy

Immunostaining was performed according to methods previously described (Hasegawa et al., 2010). The primary Abs used included anti-VPS35 (GeneTex) and anti-CI-MPR (Epitomics) Abs. Positive immunostainings were detected using Alexa 488- and Alexa 568-conjugated secondary Abs (Molecular Probes/Life Technologies). Nuclei were counterstained with the far-red fluorescent DNA dye DRAQ7™ (CST) and were pseudocolored blue. Images were analyzed with a FluoView FV300 confocal laser microscope system equipped with HeNe-Green (543 nm), HeNe-Red (633 nm) and Ar (488 nm) laser units (Olympus, Tokyo, Japan). In multi-labeling experiments, images were collected using a single excitation for each wavelength separately, and were then merged using Fluoview image analysis software (version 4.1, Olympus).

Drosophila stocks

Fly culture and crosses were performed under standard conditions at 25 °C. The fly lines bearing *elav*-GAL4, *Act5c*-GAL4, *UAS*-EGFP, *UAS*-GFP dsRNA (*GFP*-RNAi), and *UAS-h[wt]-SNCA* transgenes were obtained from the Bloomington *Drosophila* Stock Center at Indiana University (BDSC, Bloomington, IN). The *VPS35* RNAi fly lines (#45570 and #22180, designated as *dVPS35* RNAi-1 and *dVPS35* RNAi-2, respectively) were provided by the Vienna Drosophila RNAi Center (VDRC, Vienna, Austria). Tg fly lines bearing the *GMR*-GAL4 have been described previously (Yamaguchi et al., 1999).

RT-PCR analysis

Total RNA was extracted from fly heads and their cDNA was synthesized with a SuperScript® III (Life Technologies). PCR amplification of dVPS35 was performed with 1 μl of cDNA solution and PrimeSTAR Max® DNA polymerase (Takara, Tokyo, Japan) with the following primer pairs: dVps35#2-F (5′-ATGGTTTGGATGACCAGGAGAAG-3′) in exon 1 and dVps35#2-R (5′-TCGTTCTCCTCAACCATCACATC-3′) in exon 3. Human αSYN was amplified using the set of primer pairs Syn-F (5′-TCGTGAGCGGAGAACTGGGAG-3′) and Syn-R (5′-TCAAGAAACTGGGAGCAAAGAT-3′) (Hasegawa et al., 2004). To normalize sample variations, the cDNA of ribosomal protein 49 (*rp49*), a housekeeping gene, was amplified using the primer pairs rp49-F (5′-AGCGCACCAAGCACTTCATCCGCCA-3′) and rp49-R (5′-GCGCACGTTGTGCACCAGGAACTTC-3′). After amplification, 10-ml aliquots were electrophoresed on 2.5% agarose gels, followed by photographic recording of the gels stained with ethidium bromide.

Immunohistochemistry

Sections of adult fly brain were immunostained according to the methods described previously (Feany and Bender, 2000). Briefly, 4-week-old adult flies were fixed in formalin and embedded in paraffin. To assess brain morphology, 5-μm frontal paraffin sections of heads were obtained and stained with hematoxylin and eosin. To evaluate the expression of human αSYN in the fly brain, anti-syn-1 monoclonal Ab (BD Bioscience) was applied at a 1:1000 dilution. Positive signals were detected by the avidin–biotin–peroxidase complex (Vectastain Elite ABC Kit, Vector Laboratories) method as described previously. The pictures were taken with a Biozero BZ-8000 digital microscope (Keyence, Tokyo, Japan). The numbers of αSYN-positive inclusions were counted per 15 × 15 μm^2 area in a defined area of the cortex (Kenyon cells) (Chen and Feany, 2005). Eight hemibrains were examined per genotype. The pooled data were statistically evaluated by a one-way ANOVA followed by a Bonferroni multiple comparison test.

Eye images

The eye phenotypes of 4-week-old anesthetized flies were evaluated. A minimum of 25 flies were evaluated for each genotype and conditions. Scanning electron microscopic images were obtained using a Miniscope TM-1000 (Hitachi, Tokyo, Japan). For the quantification of intact bristle numbers, a high-resolution image of a compound eye was printed, and the maximal visible surface was delimited (usually 300–500 ommatidia). The number of visible interommatidial bristles was counted and divided by the total number of ommatidia (Hilgers et al.,

2010). At least 10 eyes were analyzed for each genotype. The pooled data were statistically analyzed by a one-way ANOVA followed by a Bonferroni multiple comparison test.

Climbing assay

The climbing assay was performed, with slight modifications, according to published protocols (Feany and Bender, 2000). Ten to 20 male flies were placed into a conical glass tube (length, 15 cm; diameter, 2.5 cm) without anesthesia. Ten seconds after being tapped to the bottom of the tube, the number of flies in each vertical area was counted and scored as follows: score of 0 (0–2 cm), 1 (2–3.9 cm), 2 (4–5.9 cm), 3 (6–7.9 cm), 4 (8–9.9 cm), or 5 (10–15 cm). Five trials were performed in each group at 20 s intervals and the climbing index was calculated as follows: each score multiplied by the number of flies was divided by the total number of flies, and the mean score of each trial was calculated. The results are presented as the means ± standard errors of the scores obtained in 5–7 independent experiments. All climbing assay experiments were conducted at 25 °C. Pooled data from at least five independent experiments were statistically analyzed using a two-way ANOVA with a Bonferroni multiple comparison test.

Results

VPS35 RNAi alters CI-MPR distribution and impairs maturation of CTSD

The RNAi-mediated silencing of retromer subunits, such as VPS26 and Rab7, prevents the retrieval of unoccupied CI-MPR from endosomes to the TGN, leading to the lysosomal turnover of CI-MPR and a decrease in the cellular level of lysosomal hydrolases (Rojas et al., 2008). To determine whether the depletion of VPS35 also affects the intracellular distribution of CI-MPR, we downregulated VPS35 in HEK293 cells using two different siRNAs (#1 and #2) targeting *VPS35*. Consistent with previous findings (Rojas et al., 2008), the punctate signals of CI-MPR in cells expressing a normal level of endogenous VPS35 were preferentially localized in the perinuclear space, in which the TGN and late endosomes are usually located (Fig. 1A, left inset). In contrast, the CI-MPR signals in the VPS35-deficient cells were strikingly decreased and showed a more dispersed distribution in the periphery (Fig. 1A, right inset). As shown in Fig. 1B, human CTSD is first synthesized as pre-pro-CTSD, which is further converted to pro-CTSD (52 kDa), by the removal of the signal peptide, in the endoplasmic reticulum. The transport of pro-CTSD from the Golgi to the downstream acidic compartments is mainly mediated by the M6P pathway, i.e., the M6P residues on pro-CTSD are recognized by CI-MPR in the TGN, which segregates CTSD into transport vesicles that are delivered to the late endosomes and lysosomes. In late endosomes, pro-CTSD is processed to an intermediate form (48 kDa) and subsequently converted to mature CTSD (34 kDa) in lysosomes (Laurent-Matha et al., 2006). We confirmed that the ablation of the VPS35 component of the retromer by RNAi in HEK293 cells caused a considerable increase in intracellular pro-CTSD (indicated by an *asterisk*), whereas the amount of intracellular mature CTSD (indicated by an arrowhead) was markedly decreased. Notably, these changes were accompanied by a concomitant increase in pro-CTSD in the culture medium (Fig. 1C and D). The reduction in CI-MPR expression observed in VPS35-deficient cells implies a rerouting of CI-MPR to the lysosome for degradation, which is indicative of retromer dysfunction. As suggested by previous studies, the level of VPS26, a known interaction partner of VPS35, was substantially decreased in VPS35-silenced cells. The aberrant processing of CTSD in VPS35-deficient cells was further confirmed by an enzymatic assay showing that the activity of CTSD in VPS35 siRNA-treated cells was significantly lower than that in scrambled siRNA-treated cells (Fig. 1E).

VPS35 downregulation induces the αSYN accumulation in parallel with the reduction of mature CTSD in late endosomes and lysosomes

To examine whether CTSD effectively degrades αSYN in cultured cells, we over-expressed human CTSD in HEK293 cells that constitutively expressed human αSYN. When CTSD was highly over-expressed (3 μg of plasmid DNA per transfection) for 48 h, the level of mature CTSD was increased and the signal intensity of the monomeric, full-length αSYN (17 kDa) was significantly decreased (Fig. 2A, upper panel). Notably, in the presence of the protein synthesis inhibitor cycloheximide, the effect of CTSD on αSYN degradation was augmented and the amount of αSYN was significantly decreased in proportion to the dosage of CTSD expression (Fig. 2A, lower panel). Because pro-CTSD has a relatively long half-life (3–6 h) compared to αSYN (1.84 ± 0.16 h) (Bennett et al., 1999; Capony et al., 1989), it is likely that the cycloheximide blockage of protein synthesis did not affect CTSD levels dramatically. In agreement with a previous report (Cullen et al., 2009), the decrement in the αSYN monomer level was not accompanied by the appearance of low-molecular-weight αSYN fragments even with a long exposure of the immunoblot to the synuclein-1 Ab, which had previously shown reactivity with C-terminally truncated αSYN fragments *in vivo*. We used an MTT (3-(4,5-dimethylthiazo-2-yl)-2,5-diphenyltetrazolium bromide) assay to confirm that the observed effect of CTSD on lowering αSYN expression was not caused by impaired viability of the transfected cells (data not shown). In the second set of experiments, we examined whether the reduction in mature CTSD in response to *VPS35* knockdown altered the expression level of αSYN in the HEK293 cells stably expressing HA-tagged αSYN. Remarkably, the loss of VPS35 induced the accumulation of cellular HA-αSYN concomitant with incorrect processing of CTSD (Fig. 2B). The relative decrease in MPR in VPS35-depleted cells was interpreted as compromised retromer recruitment. Because CTSD is only active in an acidic environment, such as in late endosomes and lysosomes, serial fractionation was conducted to clarify the subcellular distribution of HA-αSYN in the *VPS35*-silenced cells. Thirty-six hours after silencing, the cells were harvested and sequentially fractionated into cytosol, endosome, and lysosome fractions. All samples were subjected to an immunoblot analysis, and the relative purity of the fractions was assessed using Abs directed against specific markers including Heat shock protein 90 (HSP90; cytosol), Rab5 (early endosome), and lysosome-associated membrane protein-2 (LAMP-2; lysosome). The results, shown in Fig. 2C, revealed that after silencing *VPS35*, the expression level of CI-MPR was slightly decreased in the endosomes but simultaneously increased downstream, in the lysosomal compartment. It

Fig. 1. Silencing of VPS35 caused a reduction in CI-MPR distribution and impaired maturation of CTSD. (A) The punctate signals of CI-MPR (red) in HEK293 cells expressing a normal level of endogenous VPS35 (green) were preferentially localized in the perinuclear space (left inset). In contrast, the signal of CI-MPR in VPS35-deficient cells was strikingly decreased and had a more dispersed distribution throughout the cell (right inset). White dotted lines show the contour of the cells. Nuclei were counterstained with DRAQ7. Scale bar: 10 μm. (B) Schematic diagram of the maturation process of CTSD. Human CTSD is first synthesized as pre-pro-CTSD, which is converted to pro-CTSD (52 kDa) by the removal of the signal peptide in the endoplasmic reticulum. The transport of pro-CTSD from the Golgi to the downstream acidic compartments is mainly mediated by the CI-MPR. In late endosomes, pro-CTSD is processed to an intermediate form (48 kDa) and subsequently converted to mature CTSD (34 kDa) in lysosomes. (C) The aberrant processing of CTSD in VPS35-deficient cells. The silencing of VPS35 by two different siRNAs (#1 and #2) in HEK293 cells caused a striking increase in the intracellular pro-CTSD (asterisk), whereas the amount of intracellular mature CTSD (arrowhead) was markedly decreased. This finding was accompanied by a concomitant increase in pro-CTSD in the medium. The left inset is CTSD with a longer exposure time. The reduction in CI-MPR expression observed in VPS35-deficient cells is indicative of retromer dysfunction. Note that the level of VPS26, another component of the retromer, was substantially decreased in VPS35-silenced cells. α-Tubulin and BSA were used as the internal controls for the total cell lysate and the medium, respectively. Representative blots from five independent experiments are presented. (D) The ratio of the densitometric values of mature/pro-CTSD both in cells and the medium is presented. Data are expressed as the means ± standard errors. $^{\dagger}p < 0.05$ and $^{\ddagger}p < 0.01$ (one-way ANOVA followed by Dunnett's test; $n = 5$). (E) The activity of CTSD in VPS35-specific siRNA (#1 and #2)-treated cells significantly declined compared to the activity in scrambled siRNA-treated cells. Data are expressed as the means ± standard errors. $^{\#}p < 0.05$ (one-way ANOVA followed by Dunnett's test; $n = 5$).

should be noted that the late endosome and lysosome share many features and both endosomal and lysosomal fractions are usually positive for LAMP2. The endosomal fraction isolated by our method contains both early and late endosomes because this fraction was positive for Rab5 and LAMP-2. In this study, the Rab5-negative, LAMP-2 positive component was defined as the lysosomal fraction. These findings suggest that in VPS35-depleted cells, the retromer fails to retrieve CI-MPR from the endosomes, resulting in the accumulation of CI-MPR in the lysosomes. CTSD was detected in both the endosome and lysosome fractions in HEK293 cells. However, after *VPS35* was silenced, the level of mature CTSD was substantially decreased in the lysosomes, whereas the pro-CTSD was upregulated in the endosomes. It is also interesting to note

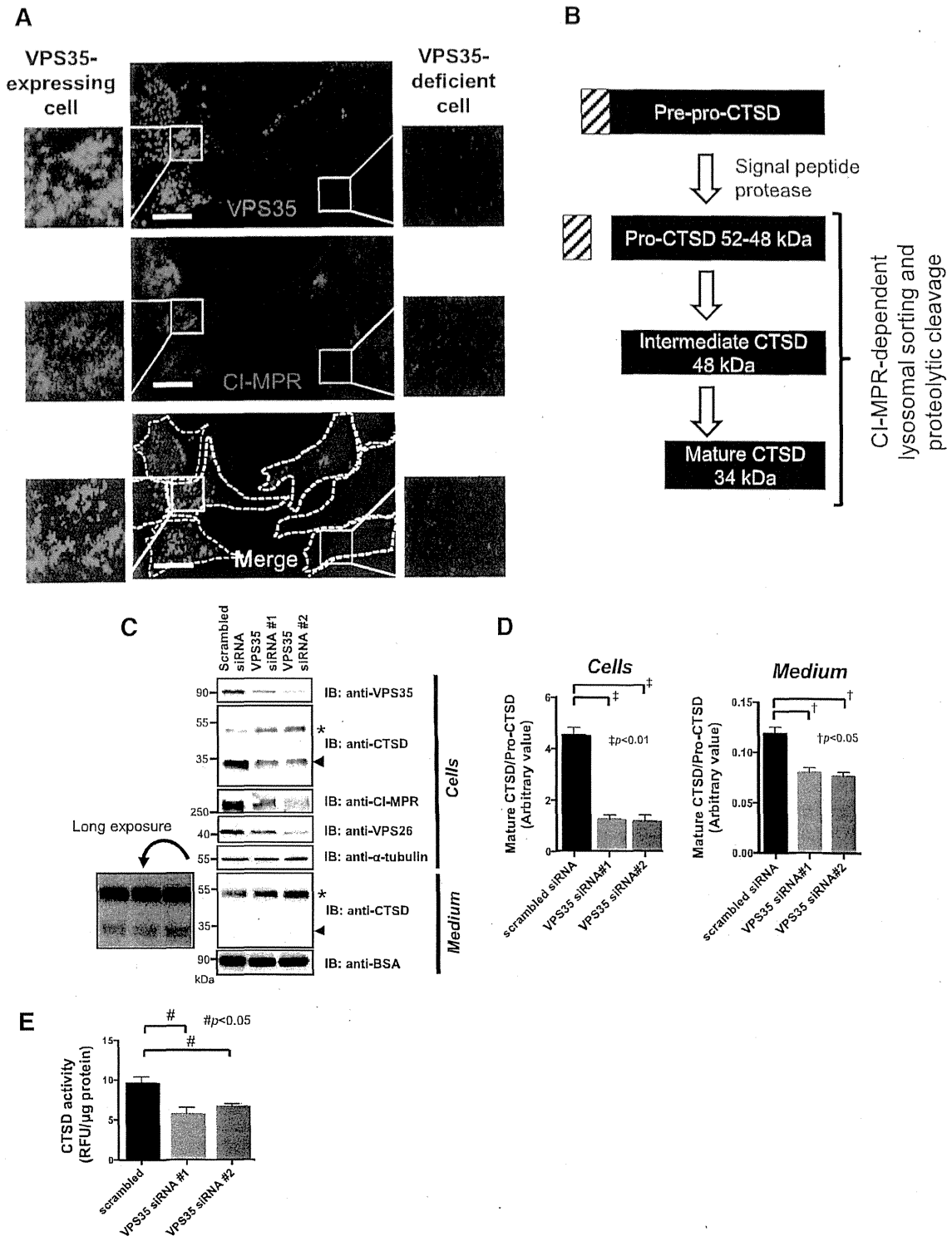

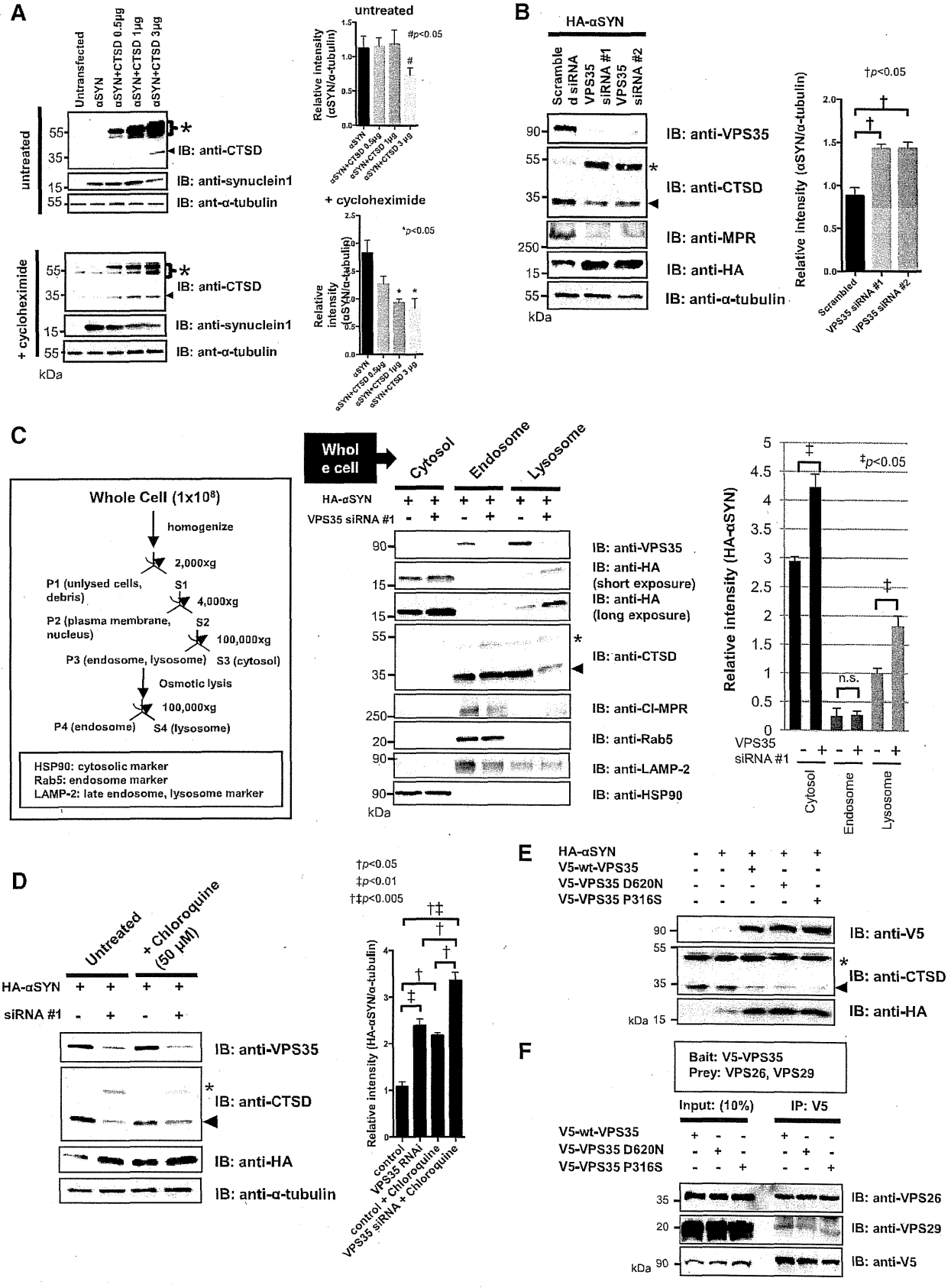
A
Untransfected
αSYN
αSYN+CTSD 0.5μg
αSYN+CTSD 1μg
αSYN+CTSD 3μg
untreated
IB: anti-CTSD
IB: anti-synuclein1
IB: ant-α-tubulin
+ cycloheximide
kDa
Relative intensity (αSYN/α-tubulin)
#p<0.05
*p<0.05
B
HA-αSYN
Scramble d siRNA
VPS35 siRNA #1
VPS35 siRNA #2
IB: anti-VPS35
IB: anti-CTSD
IB: anti-MPR
IB: anti-HA
IB: anti-α-tubulin
†p<0.05
Scrambled
VPS35 siRNA #1
VPS35 siRNA #2
C
Whole Cell (1x10⁸)
homogenize
2,000xg
P1 (unlysed cells, debris)
S1
4,000xg
P2 (plasma membrane, nucleus)
S2
100,000xg
P3 (endosome, lysosome)
S3 (cytosol)
Osmotic lysis
100,000xg
P4 (endosome)
S4 (lysosome)
HSP90: cytosolic marker
Rab5: endosome marker
LAMP-2: late endosome, lysosome marker
Whole cell
Cytosol
Endosome
Lysosome
VPS35 siRNA #1
IB: anti-VPS35
IB: anti-HA (short exposure)
IB: anti-HA (long exposure)
IB: anti-CTSD
IB: anti-CI-MPR
IB: anti-Rab5
IB: anti-LAMP-2
IB: anti-HSP90
Relative intensity (HA-αSYN)
‡p<0.05
n.s.
D
Untreated
+ Chloroquine (50 μM)
IB: anti-VPS35
IB: anti-CTSD
IB: anti-HA
IB: anti-α-tubulin
†p<0.05
‡p<0.01
†‡p<0.005
control
VPS35 RNAi
control + Chloroquine
VPS35 siRNA + Chloroquine
E
V5-wt-VPS35
V5-VPS35 D620N
V5-VPS35 P316S
IB: anti-V5
IB: anti-CTSD
IB: anti-HA
F
Bait: V5-VPS35
Prey: VPS26, VPS29
Input: (10%)
IP: V5
IB: anti-VPS26
IB: anti-VPS29
IB: anti-V5

that treatment with chloroquine, a lysosomotropic agent that prevents endosomal acidification, further augmented the accumulation of HA-αSYN by VPS35 RNAi (Fig. 2D). This indicates that VPS35 knockdown does not completely inhibit lysosomal αSYN degradation. These observations indicate that if the retromer machinery is compromised, the pro-CTSD is entrapped in upstream structures and cannot be properly transported to the downstream acidic compartment. In an inverse correlation with the level of mature CTSD, the level of HA-αSYN was substantially upregulated in the lysosome fraction and the cytosol in the *VPS35*-silenced cells. Since autophagosomes should engulf cytosolic αSYN (Vogiatzi et al., 2008), increased cytosolic αSYN can be interpreted as the result of insufficient autophagic/lysosomal clearance of αSYN. To determine the possible effects of PD-linked mutations of *VPS35* on retromer function and αSYN degradation, we co-expressed HA-αSYN and mutant VPS35 (D620N and P316S) in HEK293 cells. Surprisingly, the over-expressed wt and the mutant VPS35 led to an equal αSYN accumulation, with no significant difference in the impaired maturation of CTSD (Fig. 2E). Furthermore, coimmunoprecipitation analyses of the wt and mutant VPS35 detected no differences in the binding affinity toward its known binding partners, VPS26 and VPS29 (Fig. 2F). Together, these findings indicate the essential role of the retromer machinery in lysosomal CTSD function in regulating the proteolytic pathway that is important for αSYN metabolism.

RNAi-mediated silencing of dVPS35 not only increased the insoluble αSYN species in brain but also deteriorated eye organization and locomotor function in human αSYN transgenic Drosophila

Although the retromer is implicated in PD pathogenesis, there is no evidence showing that deficiencies in the retromer sorting pathway cause the key phenotypes of the disease. Because the retromer complex is highly conserved and homologs have been found in yeast, nematode, fly, mouse, and human (Korolchuk et al., 2007), we investigated the effects of endogenous VPS35 on αSYN-induced neurotoxicity using flies that express the *h[wt]-SNCA* and *dVPS35* RNAi transgenes. The sequence-specific silencing of *dVPS35* in the fly brain was confirmed by RT-PCR (Fig. 3A). We found that the silencing of *dVPS35* strikingly increased the amount of the Triton-insoluble high-molecular-weight (HMW) αSYN species accompanied by a concomitant reduction in the level of Triton-soluble αSYN monomer in the brains of human αSYN-expressing flies under the panneural *embryonic lethal abnormal vision* (*elav*)-*GAL4* driver (Fig. 3B). This finding is well corroborated by the immunohistochemical findings showing that the numbers of αSYN-positive inclusions in the fly cortex (Kenyon cells) were significantly increased in the brain of VPS35-deficient flies compared to controls (Fig. 3C). We attempted to detect human αSYN in the fly brain with or without proteinase K treatment, but did not observe a significant difference (data not shown). The mRNA levels in the brain of 4 fly lines were analyzed by RT-PCR (Fig. 3D). Note that the transcript levels of *h[wt]-SNCA* versus *rp49* were statistically identical between the *h[wt]-SNCA* × *GFP* RNAi and *h[wt]-SNCA* × *dVPS35* RNAi-1 fly lines. Furthermore, the cathepsin D activity in the brain was significantly decreased in *dVPS35* depleted flies (Fig. 3E). We then analyzed the eye phenotypes of flies expressing αSYN under the eye-specific *glass multiple reporter* (*GMR*)-*GAL4* driver (Fig. 4A and B). When *dVPS35* was silenced, the human αSYN-Tg flies showed a slight shrinkage of each ommatidium with the loss of interommatidial bristles compared to control flies expressing both *h[wt]-SNCA* and *GFP* RNAi or both *EGFP* and *dVPS35* RNAi. We then investigated the impact of *dVPS35* silencing on the motor performance of flies that over-expressed human αSYN in the nervous system. For this purpose, we utilized a simple but powerful behavioral assay: the climbing assay. As shown in Fig. 5A and B, the flies overexpressing human wt-αSYN with *dVPS35* RNAi (*dVPS35* RNAi-1 and *dVPS35* RNAi-2) showed a significant, age-dependent deterioration in climbing ability compared to those expressing *GFP*-RNAi. Note that the flies that expressed αSYN in the absence of *dVPS35* did not have a shortened life span compared to the control flies (data not shown).

Discussion

In this study, we first showed that the silencing of *VPS35* in cultured cells caused a reduction in the distribution of CI-MPR and impaired the maturation of CTSD. Second, we found that the amount of pro-CTSD was substantially increased in the culture medium of the VPS35-deficient cells. Third, we demonstrated that silencing *VPS35* impairs the maturation of CTSD, which occurs concomitant with a striking accumulation of αSYN in lysosomes. Finally, we showed that the RNAi-mediated silencing of *dVPS35* not only induced the accumulation of the detergent-insoluble αSYN species in the brain but also exacerbated mild eye disorganization, as well as causing locomotor impairment in the flies expressing the human wild-type αSYN. Cumulatively, these data suggest that the retromer-dependent sorting machinery plays a role in αSYN catabolism by modulating the intracellular processing and activation of CTSD and might thereby contribute to the pathogenesis of PD (Fig. 6).

Although the evidence suggests that VPS35 is involved in the pathogenesis of PD, the mechanisms by which the mutant VPS35 causes retromer dysfunction and the subsequent neurodegeneration remain elusive. Given that the expression of VPS35 is significantly decreased in the brain regions selectively vulnerable to PD and AD and the studies in animal models (MacLeod et al., 2013; Muhammad et al., 2008; Small et al., 2005; Wen et al., 2011), the loss-of-function mechanism may explain the VPS35-related defective vesicle trafficking and subsequent neurodegeneration. As suggested by previous studies, our immunoprecipitation analyses indicate that the over-expressed VPS35 mutants (D620N and P316S) seem to maintain the binding capacity for the retromer subunits VPS26 and VPS29 (Vilarino-Guell et al., 2011). Nevertheless, the expression of the yeast VPS35 mutation (p.R98W) in the

Fig. 2. VPS35 depletion impairs the maturation of CTSD concomitantly with the accumulation of αSYN mainly in the late endosomes and lysosomes. (A) The level of exogenously expressed human αSYN (17 kDa) in HEK293 cells was decreased when the CTSD was highly over-expressed (3 μg plasmid for transfection) for 48 h (upper panel). Notably, under the existence of protein synthesis inhibitor cycloheximide, the effect of CTSD on αSYN degradation was augmented and the amount of αSYN was significantly decreased in proportion to the dosage of CTSD expression (lower panel). Pro-CTSD and mature CTSD are indicated by an asterisk and an arrowhead, respectively. Representative immunoblots from three independent experiments are shown. The densitometric quantification of αSYN versus α-tubulin is presented in the right panel. Data are expressed as the means ± standard errors. $^{\#,*}p < 0.05$ (one-way ANOVA followed by Dunnett's test; $n = 5$). (B) The depletion of VPS35 by siRNA (#1 and #2) induced the accumulation of intracellular HA-αSYN concomitant with the incorrect processing of CTSD in HEK293 cells stably expressing HA-αSYN. Pro-CTSD and mature CTSD are indicated by an asterisk and an arrowhead, respectively. Retromer dysfunction in VPS35-deficient cells was confirmed by the reduction in CI-MPR expression. Representative immunoblots from three independent experiments are presented. The relative band intensity of αSYN versus α-tubulin was calculated and is presented in the right panel. Data are expressed as the means ± standard errors. $^{\dagger}p < 0.05$ (one-way ANOVA followed by Dunnett's test; $n = 5$). (C) A marked increase in HA-αSYN in the lysosome fraction, as well as the cytosol, in *VPS35*-silenced HEK293 cells expressing HA-αSYN. Note that the expression level of CI-MPR was slightly decreased in the endosomes but simultaneously increased in the downstream lysosome compartments. CTSD was detected both in the endosome and lysosome fractions in HEK293 cells; however, after silencing *VPS35*, the level of mature CTSD (arrowhead) was substantially decreased in the lysosomes, whereas the pro-CTSD (asterisk) appeared upregulated in the endosomes. HSP90, Rab5, and LAMP-2 were used as the subcellular markers for the cytosol, endosome, and late endosome/lysosome, respectively. The fractionation and immunostaining were performed five times and exhibited consistent results. The densitometric quantification of HA-αSYN in each fraction is presented in the right panel. Data are expressed as the means ± standard errors. $^{\ddagger}p < 0.05$ (unpaired Student's *t*-test; $n = 5$). (D) Treatment with the lysosomal inhibitor, chloroquine (50 μM for 5 h), significantly augmented the accumulation of HA-αSYN by VPS35 RNAi. The relative band intensity of HA-αSYN versus α-tubulin is presented in the right panel. Data are expressed as the means ± standard errors. $^{\dagger}p < 0.05$ and $^{\ddagger}p < 0.01$ (one-way ANOVA followed by Dunnett's test; $n = 5$). (E) The over-expressed wt as well as mutant VPS35 in HEK293 cells equally led to αSYN accumulation, with no significant difference in the impaired CTSD maturation. (F) Coimmunoprecipitation analyses using HEK293 cells co-expressing wt and the mutant VPS35 detected no difference in the binding affinity toward its known binding partners, VPS26 and VPS29. Experiments were performed 3 times and yielded similar results.

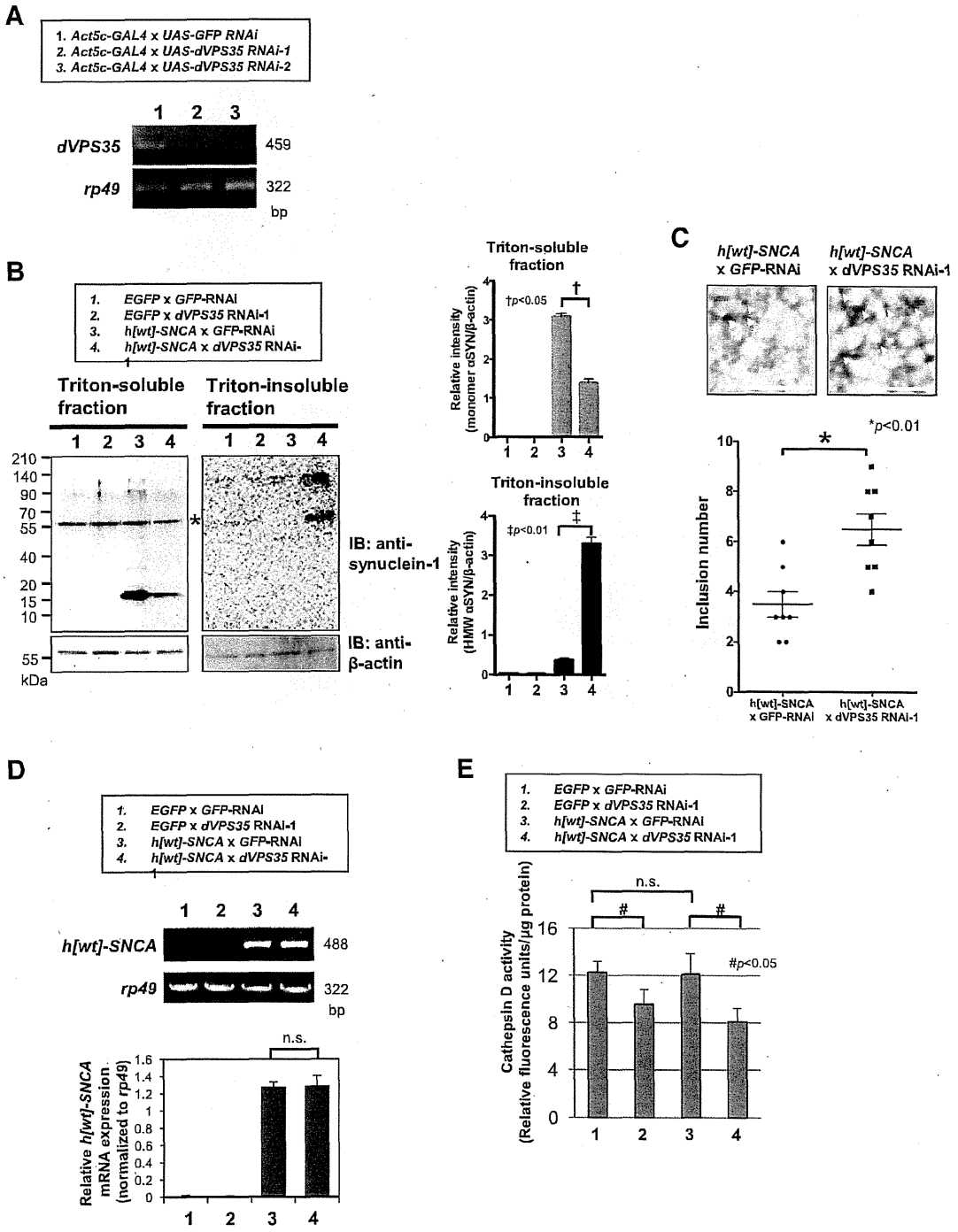

Fig. 3. Knockdown of *dVPS35* in human αSYN transgenic *Drosophila*. (A) Generation of *dVPS35*-knockdown flies. The sequence-specific silencing of *dVPS35* in the fly brain was confirmed by RT-PCR analysis. Ribosomal protein 49 (*rp49*), a housekeeping gene, was used as an internal control. RNAi-mediated knockdown was induced by *Act5c-GAL4*, which expresses GAL4 ubiquitously. (B) Neuron-specific knockdown of *dVPS35* affects the catabolism of the human wt αSYN. The *elav*-GAL4 driver was used for the transgene expression. Note that the silencing of *dVPS35* strikingly increased the amount of Triton-insoluble HMW αSYN species, which was accompanied by the concomitant reduction in Triton-soluble αSYN monomer in the brains of human αSYN-expressing flies under the *elav*-GAL4 driver. Equal loading was confirmed by an immunoblot using a β-actin Ab. An asterisk indicates the unspecific band that emerged due to the synuclein-1 Ab. The normalized band intensity data of monomeric αSYN in the Triton-soluble fraction (gray bar) as well as the HMW αSYN (above 100 kDa) in the Triton-insoluble fraction (black bar) are presented in the right panel. Data are expressed as the means ± standard errors. $^{\dagger}p < 0.05$ and $^{\ddagger}p < 0.01$ (one-way ANOVA followed by Dunnett's test; $n = 5$). (C) The immunohistochemical staining of fly brains using a human αSYN-specific antibody. The αSYN-positive inclusions (arrowhead) were counted in a defined area of the cortex (Kenyon cell). Note that the numbers of αSYN-positive inclusions in the fly cortex were significantly increased in the brain of VPS35-deficient flies compared to controls. Scale bar: 10 μm. (D) The mRNA levels in the brains of 4 fly lines were analyzed by RT-PCR. *Rp49* was used as an internal control. Note that the transcript levels of *h[wt]-SNCA* are statistically identical between the *h[wt]-SNCA* × *GFP* RNAi and *h[wt]-SNCA* × *dVPS35* RNAi-1 fly lines. The relative *h[wt]-SNCA* mRNA expression levels normalized to *rp49* were calculated. Data are expressed as the means ± standard errors (one-way ANOVA followed by Dunnett's test; $n = 5$). (E) The CTSD activity in the brain was significantly decreased in *dVPS35* depleted flies. Results are presented as means ± standard errors. $^{\#}p < 0.05$ (one-way ANOVA with the post-hoc Dunnett's test; $n = 5$).